Alcohol reverses the effects of *KCNJ6* (GIRK2) noncoding variants on excitability of human glutamatergic neurons

Running title: Alcohol reverses effects of *KCNJ6* variants on neurons

Dina Popova[1], Isabel Gameiro-Ros[2], Mark M. Youssef[3], Petronio Zalamea[1], Ayeshia D. Morris[4], Iya Prytkova[2], Azadeh Jadali[3], Kelvin Y. Kwan[3], Chella Kamarajan[5], Jessica E. Salvatore[6], Howard J. Edenberg[7], Xiaoling Xuei[8], David B. Chorlian[5], Bernice Porjesz[5], Samuel Kuperman[9], Danielle M. Dick[10], Alison Goate[11], Jay A. Tischfield[1], Zhiping P. Pang[1,12], Paul A. Slesinger[2] and Ronald P. Hart[1,3,*]

Affiliations:

[1]Human Genetics Institute, Rutgers University, Piscataway, NJ 08854
[2]Nash Family Department of Neuroscience, Icahn School of Medicine at Mount Sinai, New York, NY 10029
[3]Department of Cell Biology & Neuroscience, Rutgers University, Piscataway, NJ 08854
[4]Joint Program in Toxicology, Rutgers University, Piscataway, NJ 08854
[5]Dept. of Psychiatry & Behavioral Sciences, SUNY Downstate Health Sciences University, Brooklyn, NY 11203
[6]Department of Psychiatry, Rutgers Robert Wood Johnson Medical School, Rutgers University, Piscataway, NJ 08854
[7]Department of Biochemistry and Molecular Biology, Indiana Univ School of Medicine, Indianapolis, IN 46202
[8]Department of Medical and Molecular Genetics, Indiana University School of Medicine, Indianapolis, IN 46202
[9]Department of Psychiatry, University of Iowa Carver College of Medicine, Iowa City, IA 52242
[10]Rutgers Addiction Research Center, Robert Wood Johnson Medical School, Rutgers University, Piscataway, NJ 08854
[11]Department of Genetics & Genomic Sciences, Icahn School of Medicine at Mount Sinai, New York, NY 10029
[12]Child Health Institute, Robert Wood Johnson Medical School, Rutgers University, New Brunswick, NJ 08854

*Corresponding author:
Rutgers University
Department of Cell Biology & Neuroscience
604 Allison Rd
Piscataway, NJ 08854

(848) 445-1783
rhart@rutgers.edu

Abstract

Synonymous and noncoding single nucleotide polymorphisms (SNPs) in the *KCNJ6* gene, encoding G protein-gated inwardly rectifying potassium (GIRK2) channel subunit 2, have been linked with increased electroencephalographic frontal theta event-related oscillations (ERO) in subjects diagnosed with alcohol use disorder (AUD). To identify molecular and cellular mechanisms while retaining the appropriate genetic background, we generated induced excitatory glutamatergic neurons (iN) from iPSCs derived from four AUD-diagnosed subjects with *KCNJ6* variants ('Affected: AF') and four control subjects without variants ('Unaffected: UN'). Neurons were analyzed for changes in gene expression, morphology, excitability and physiological properties. Single cell RNA sequencing suggests that *KCNJ6* AF variant neurons have altered patterns of synaptic transmission and cell projection morphogenesis. Results confirm that AF neurons express lower levels of GIRK2, have greater neurite area, and elevated excitability. Interestingly, exposure to intoxicating concentrations of ethanol induces GIRK2 expression and reverses functional effects in AF neurons. Ectopic overexpression of GIRK2 alone mimics the effect of ethanol to normalize induced excitability. We conclude that *KCNJ6* variants decrease GIRK2 expression and increase excitability and that this effect can be minimized or reduced with ethanol.

Teaser

In human neurons made from stem cells, noncoding *KCNJ6* gene variants alter excitability, which is reversed with ethanol.

Introduction

Alcohol use disorder (AUD) is a heritable (h^2 = 0.49) condition characterized by an impaired ability to stop or control alcohol use despite adverse social, occupational, or health consequences (*1*). An estimated 14.1 million American adults (ages 18+) were diagnosed with AUD in 2019 and the numbers continue to grow, particularly due to the COVID-19 pandemic (*2*). Even though several evidence-based treatments are available for AUD (*3-5*), there is a high discrepancy in treatment outcomes, suggesting the existence of a variety of traits influencing the development of specific physiological and behavioral responses to alcohol. Understanding biological factors, specifically genetic risk, at the level of neuronal function is fundamental to developing tailored preventive interventions and better matching of patients to treatment.

The Collaborative Study on the Genetics of Alcoholism (COGA) collected a diverse set of phenotypes, including electroencephalogram (EEG) parameters, in the search for genes and endophenotypes associated with AUD (*6, 7*). A family-based, genome-wide association study (GWAS) of a frontal theta event related oscillation (ERO) phenotype identified an association with several single nucleotide polymorphisms (SNPs), including a synonymous SNP, rs702859, in the *KCNJ6* gene on chromosome 21 (*8*). More recent studies concluded that the rs702859 polymorphism influences the magnitude and topography of ERO theta power during reward processing in a monetary gambling task, reflecting a genetic link to neuronal circuits (*9, 10*). Two other SNPs (rs702860 and rs2835872) within *KCNJ6* were linked with the ERO endophenotype and AUD, but are noncoding, either intronic or within the 3' untranslated region (3' UTR), respectively. Additional studies identified various genetic loci correlating with selected EEG results but all consistently include alcohol dependence (*11, 12*). To understand how these SNPs might influence these phenotypes, it is essential to characterize the pathways and mechanisms by which genetic risk unfolds at molecular, cellular and network resolutions. Furthermore, since the *KCNJ6* SNPs are non-coding or synonymous, the optimal strategy would incorporate human genetic backgrounds of actual subjects to preserve potential effects of noncoding sequences.

KCNJ6 encodes the G protein-gated inwardly rectifying potassium channel subunit 2 (GIRK2), which, when assembled into a GIRK channel, plays a role in regulating cell excitability (*13*). The inward rectifying properties of GIRK are based on the ability to conduct potassium ions into the cell more easily than out, leading to a reduction in excitability (*14, 15*). GIRK function in neurons is associated with activation of G protein-coupled receptors (GPCRs), which leads to dissociation of Gβγ subunits from the G protein complex and binding to the channel (*16*). In addition, this family of GIRK channels can be potentiated by ethanol concentrations (20-50 mM) relevant to human alcohol usage through direct interaction with a hydrophobic pocket on the channel (*17, 18*). Studies in model organisms also reveal the importance of GIRK function in AUD: mice lacking GIRK2 demonstrate reduced ethanol analgesia, greater ethanol-stimulated activity in open-field tests, increased self-administration of ethanol, and failure to develop a conditioned place preference for ethanol (*19-21*). Thus, GIRK channels not only modulate the excitability of the neurons but also play an essential role in regulating responses to alcohol.

Recent studies have employed the use of subject-specific induced stem cell technology to model, characterize and elucidate mechanisms underlying various types of addiction disorders including AUD (*22-25*). The generation of specific subtypes of cultured human neurons enables the study of formerly inaccessible functional properties using standard neuroscience methods (*22, 24-26*). The contribution of various *KCNJ6* SNPs was found to affect a variety of properties associated with neuronal function or sensitivity to drugs of abuse, suggesting targets for potential therapeutic interventions. Associating specific genetic variants with mechanisms contributing to addictive behaviors may produce more effective therapies tailored to individual genotypes.

We hypothesize that noncoding SNP variants in *KCNJ6* alter neuronal excitability, potentially contributing directly or indirectly to network-level endophenotypes such as ERO. Furthermore, since ethanol interacts directly with GIRK2, we predict that excitability will be modulated by ethanol. To test these hypotheses, we evaluated a human neuron model system that includes variant genotypes, so that specific intergenic or noncoding sequences as well as modifying genetic background influencing these functions would be preserved. Therefore, we selected subjects from the NIAAA/COGA Sharing Repository, four with the ERO-associated allelic variant in *KCNJ6* and the presence of diagnosed alcohol dependence and four without the variant and unaffected for AUD and produced eight iPSC lines. iPSCs were reprogrammed into excitatory human neurons (iN) to investigate the potential contribution of the *KCNJ6* SNPs to AUD diagnosis and the ERO power endophenotype (Fig. 1A). We found that neurons from *KCNJ6* variant AUD-affected individuals demonstrated initial transcriptomic and morpho-physiological differences, mostly affecting excitability of the cells, which were paralleled by differences in GIRK2 expression levels. Ethanol exposure, conversely, induced GIRK2 expression, ameliorating differences in excitability. Moreover, by overexpressing *KCNJ6* we replicated effects of ethanol on neuronal excitability. The results promote a better understanding of the association between genetic variants and brain-wide changes affecting AUD risk and can potentially be used for development of personalized interventions.

Results

Gene expression patterns predict functional differences between iN generated from AUD affected and unaffected individuals

To investigate the role of *KCNJ6* gene variants in neuronal function and ethanol response we selected a balanced set of eight subjects of European ancestry from the COGA cell repository, with contrasting *KCNJ6* SNPs and the presence or absence of alcohol dependence (Table 1). Since multiple SNP genotypes were used, we label groups as AUD "affected" (**AF**) or "unaffected" (**UF**) for simplicity, since in this set of subjects diagnosis correlates with the SNP haplotype. However, the focus of this study is the *KCNJ6* haplotype.

To identify gene expression differences between the two groups, iN cultures from each cell line were harvested for bulk RNAseq analysis. Top differentially expressed genes were predominantly consistent with dissimilarities in differentiation status among cultures (Supplemental Fig. 2). Previous functional studies suggested that iN cultures were somewhat heterogeneous, potentially confounding a bulk RNAseq analysis (*27*). However, these results could be used to confirm and extend the *KCNJ6* SNP haplotype. Genome-aligned RNAseq data identified only the longer *KCNJ6* transcript isoform ENST00000609713 (Fig. 1D), which includes a 3' exon of 18,112 nucleotides that primarily consists of noncoding 3'UTR. Genotypes for the two exonic SNPs (Table 1) were confirmed for all eight cell lines, but we also identified an additional 19 noncoding, 3'UTR SNPs linked with the initial three (Supplementary Table 1; mapped with red lines in Fig. 1B), constituting a haplotype of 22 variants (synonymous and noncoding) within the expressed isoform of *KCNJ6* mRNA, all in a region of linkage disequilibrium (LD; Supplemental Figure 1C). There are no nonsynonymous variants in either haplotype, therefore, any function would be predicted to affect *KCNJ6* mRNA stability, translation, or other post-transcriptional processes.

Group	ID	Sex	DSMIV Dx	rs702859 Synonymous	rs702860 Intronic	rs2835872 Intronic
AF	376	M	Affected	GG	GG	AA
	246	M	Affected	GG	GG	AA
	351	F	Affected	GG	GG	AA
	233	F	Affected	GG	GG	AA
UN	472	M	Unaffected	AA	AA	GG
	384	M	Unaffected	AA	AA	GG
	451	F	Unaffected	AA	AA	GG
	420	F	Unaffected	AA	AA	GG

Table 1. Subjects selected for iPSC. The ID is a three-digit code that is not traceable to the subject identity. Genotypes for listed SNPs were obtained from GWAS studies (*8*).

To enable selective analysis of the more appropriately induced neurons, we used single-cell RNAseq (scRNAseq) of pooled neurons from multiple cell lines, a strategy known as a "cell village" (*28*). Based on preliminary results indicating differences in synaptic activity, we cultured each group separately, to avoid potential secondary effects due to differential synaptic activity,

combining cells from all 4 lines within each group in equivalent proportions. Following maturation (~30 days after induction), dissociated cells were processed to generate scRNAseq libraries. Mapping cells by t-distributed stochastic neighbor embedding (tSNE), a distinct cluster of cells coordinately expressed several markers consistent with neuron physiological function (Fig. 1C and Supplemental Fig. 1D), including synaptic marker (*SYP*), voltage-gated sodium channel (*SCN3A*), glutamate transporter (*SLC17A6*), and both NMDA (*GRIN2A*, *GRIN2B, GRIA2, GRIA4*) and kainate glutamate receptors (*GRIK2*). This cluster also expressed both *KCNJ6*, encoding GIRK2, and *KCNJ3*, encoding GIRK1, which are required to form heterotetrameric, functional channels (*14, 29*). Detection of mRNA expression in individual cells by scRNAseq is likely an underestimate due to the relatively small number of reads per cells, so the cluster identified as neurons is likely to express markers more uniformly than observed here. We conclude that this subset of cells represents those expressing components required for neuron physiological activity, and that other, sporadic cells, expressing subsets of these neuronal markers, are likely alternate products of induction, which we label as "transitional" neurons, since reprogramming does not fully recapitulate differentiation (Fig. 1C) (*30, 31*). Therefore, we focused gene expression analysis on the more successfully reprogrammed subset of cells.

Cells from individual subjects were distinguished by expressed SNP profiles (*32*), and sequencing reads of cells from each subject were combined to create a "pseudo-bulk" analysis, treating each subject and treatment condition as a single replicate. Comparing the untreated AF group with the untreated UN group, we identified 797 genes up-regulated, and 596 genes down-regulated (Fig. 1D; Supplemental Table 2). Gene ontology analysis of the down-regulated genes (Fig. 1E; Supplemental Table 3-4) predicts several biological processes associated with nervous system development, axonal transport, trans-synaptic signaling and others. By grouping enriched gene ontology terms into a tree plot by their parent terms (Supplemental Fig. 4), the major themes in the down-regulated genes (AF < UN; Supplemental Table 4) are synaptic signaling and neuro projection morphogenesis. Up-regulated genes (AF > UN; Fig. 1E; Supplemental Table 3) predict functions associated with protein targeting within the cells, catabolic metabolism, and nonsense-mediated decay. The level of *KCNJ6* mRNA trended lower in untreated AF than in UN (Fig. 1C; $p = 3.15 \times 10^{-5}$ by LRT over both genotype and ethanol treatment; $p = 0.0508$ for untreated AF vs. UN by Wald test). Interestingly, 7 d of 20 mM IEE increased levels of *KCNJ6* mRNA (Fig. 1C; $p = 0.0225$, Wald test) so that the treated AF group was no longer different from untreated UN ($p = 0.322$; Wald test). Results indicate that the variant *KCNJ6* haplotype leads to differential expression of GIRK2 and that ethanol exposure will reverse these effects.

GIRK2 expression and function in iPSC-derived induced excitatory human neurons (iN)

Given the differences in gene expression and partial reversal of KCNJ6 downregulation, we evaluated detailed neuronal phenotypes in UN and AF iN cultures, including GIRK2 expression, neuronal morphology, and physiological response. Since GIRK2 immunocytochemistry had not been reported in cultured human neurons, we validated detection using mouse primary cortical cultures (*33*). GIRK2 immunoreactivity in human iNs matched a pattern of process-selective expression in mouse (Fig. 2A), where GIRK2 was detected as relatively small (~ 0.5 µm diameter)

puncta scattered primarily along the processes (Fig. 2B). Localization of GIRK2 immunoreactivity in human iN did not directly colocalize with synaptic vesicle marker VGLUT2 or synaptic marker Syn1 (Supplemental Fig. 6), but instead was found most frequently adjacent to synapses but overlapping the shafts of the βIII tubulin-positive processes, and less so on MAP2 positive processes (Figs. 2D.a, 3C, 3E). Cultured neurons express βIII tubulin throughout the cell, but not as strongly in axonal processes (*34*). We previously found that processes in human iN cells stained for ankyrin G, identifying the axonal initial segment, which similarly lacked βIII-tubulin (*35*). Detection of GIRK2 primarily on βIII-tubulin$^+$/MAP$^-$ processes, therefore, suggests pre-axonal, and likely presynaptic, localization. Results confirm that lentiviral-transduced GIRK2 overexpression increased levels of immunostaining about 3.5-fold (Fig. 2C, mCherry$^+$ cells) while CRISPR/Cas9 frameshift deletions eliminate GIRK2 detection (Fig. 2C, cells without mCherry) which further confirms antibody specificity.

To confirm that GIRK2 expression contributes to potassium channel function, we treated iN cultures with ML297, a selective activator of the GIRK1/GIRK2 heterotetramer complex (*36, 37*). Results show that the magnitude and frequency of native (basal) currents observed in human iN were relatively small (Fig. 2D.b), with only 6.8% of the neurons responding to a shift in membrane potential holding current (~10 pA). This agrees well with immunocytochemical data showing that GIRK2 expression is relatively low and with scRNAseq detection of *KCNJ6* in a subset of cells (Fig. 1C). However, by recording from cells overexpressing GIRK2 (identified by mCherry co-expression; Fig. 2D.c), we found an increased frequency of response (GIRK currents) to 30% of the cells after ML297 addition (Fig. 2D.b) without a change in magnitude (Fig. 2D.e). Importantly, we also found that GIRK activation affected excitability of the neurons by shifting resting membrane potential to more negative values (Fig. 2D.d), thus affecting the ability of neurons to fire APs when induced (Fig. 2D.f). We conclude that increased *KCNJ6* expression affects neuronal excitability by altering GIRK channel activity.

KCNJ6 haplotype alters morphology and membrane excitability in human iNs

To identify neuronal properties affected by *KCNJ6* haplotype, we focused on three aspects: morphology, expression of GIRK2, and basal physiological properties. Most measures of basic neuronal morphology did not exhibit statistically significant differences by group, including soma size, circularity, and solidity, which describe the most fundamental aspects of neuron shape (Fig. 3B.a-c). However, neurite area, as determined by βIII-tubulin-stained area, reflecting the number and/or branching of neurites per cell, increased in the AF group ($p = 0.00008$; Fig. 3B.d), with example images shown for individual cell lines in Figure 3C. Results are plotted for each cell line or aggregated by *KCNJ6* haplotype from multiple cell lines. As predicted by the scRNAseq expression of *KCNJ6* mRNA (Fig. 1J), GIRK2 immunoreactivity was decreased in the AF group (Fig. 3D), as measured by puncta counts ($p = 0.0434$; Fig. 3D.a), puncta circularity ($p = 0.00295$; Fig. 3D.d), and solidity ($p = 0.0270$; Fig. 3D.e) but not puncta size (Fig. 3D.c). Sample GIRK2 puncta are shown for each cell line in Figure 3E. These results demonstrate an overall decrease in GIRK2 in neuronal processes in the AF (*KCNJ6* variant allele) group.

Reduced GIRK2 expression is predicted to affect the excitability of neurons. As expected, we found no differences in membrane capacitance, membrane resistance, spontaneous excitatory post-synaptic potential (sEPSC) frequencies or amplitudes, or spontaneous action potential (AP) firing (Fig. 3F). However, we observed a significant increase in excitability in the AF group ($p = 3.3 \times 10^{-5}$, Fig. 3G). Less current injection, using a ramp technique, was required for the AF group to shift the resting membrane potential (RMP) of neurons held at -65 mV, producing more AP firing, compared with the UN group ($p = 2.0 \times 10^{-9}$, Fig. 3G.d). Therefore, the *KCNJ6* variant haplotype group (AF) exhibited increased neurite area, reduced neurite GIRK2 expression, and greater excitability. Other neuronal properties were not different across the two groups, suggesting that overall neuron differentiation status was similar.

Electrophysiology was assessed in multiple individual cells, but since cultures are heterogeneous (Fig. 1C), we wished to evaluate larger samples of cultures. Therefore, to confirm that the observed effects are consistent across larger populations of cells, we used calcium imaging to assess spontaneous and glutamate-stimulated firing. We selected four cell lines for these studies (AF: 233 and 246, and UN: 420 and 472) and used the viral-transduced, genetically-encoded calcium indicator GCaMP6f as a proxy for neuronal activity (*38*). Example images show consistent expression in all cell lines (Fig. 4A). Cultures were treated with repeated pulses of 10 μM glutamate (each followed by wash-out with ACSF), and one pulse of 50 μM glutamate to elicit transient increases in fluorescence, indicating receptor-induced excitability, followed by pulses of 18 mM KCl, indicating cellular excitability (Fig. 4B-D). Neurons from both UN and AF groups had heterogeneous spiking patterns, with >50% of the neurons remaining inactive during the baseline period or after stimulation with glutamate or KCl. This is consistent with scRNAseq results indicating that only ~23% of the iN cells express genetic markers consistent with excitability (Fig. 1C). Increased spontaneous and induced spiking (> 1-2 spikes) was apparent in the AF group when viewing individual cell responses in a raster plot (Fig. 4B-C). Spiking frequencies increased 2.4-fold in baseline conditions (Fig. 4E; $p = 1.1 \times 10^{-6}$) and 1.3-fold following glutamate stimulation (Fig. 4F; $p = 1.6 \times 10^{-3}$) in the AF group, but no difference was found in KCl-induced activity (Fig. 4G; $p = 0.85$), confirming the above results from individual neurons. When examining the AF or UN neurons individually, we also observed higher spontaneous and glutamate elicited excitability for lines 233 and 246 when compared to line 472, which was found to be the least active spontaneously or under glutamate stimulation among the four studied with this imaging approach (Supp. Fig. 8). Overall, cells from the AF *KCNJ6* variant allele group were more excitable, with no difference in basal physiological properties (i.e., KCl-induced activity). Furthermore, not only did the spike rate increase per cell (bar plots, Spikes/ROI/min), but we also observed increases in the proportion of cells in a field that responded (pie plots). These results not only confirm earlier findings of differences in excitability, but also demonstrate that the difference in the AF iNs is found in not only individual cell activity but also in the frequency of detecting active cells within a population.

Ethanol exposure eliminates differences in neuronal properties affected by *KCNJ6* haplotype

Analysis of *KCNJ6* mRNA expression in selected neurons (Fig. 1C) not only detected decreased basal levels in the AF group, but also demonstrated increased expression following ethanol treatment (~2-fold increased, p = 0.0225 Wald test). This result predicts that increasing GIRK2 expression in the AF group following ethanol treatment would eliminate differences from the UN group in morphology, expression, and physiology.

To control ethanol dosage in culture, we utilized an intermittent ethanol exposure (IEE) paradigm as in previous studies (*25*). We replenished ethanol daily to account for loss by evaporation, producing measured concentrations with a mean of 15.4 ± 1.16 mM (Supplemental Fig. 8). We determined that the half-life of ethanol is 14.5 h (with a 95% CI of 13.5 to 15.6 h), so over 24 h the concentration would drop to ~5-8 mM before replenishment. We targeted a peak concentration of 20 mM ethanol, which is similar to a blood alcohol concentration (BAC) of 0.08% (17 mM), the legal limit for intoxication. We also selected this concentration based on the reported concentration-dependent interaction of GIRK2 with ethanol (*17*). After 7 days of IEE, we evaluated neuronal morphological and functional properties. Focusing on those parameters that were different by genotype without IEE (Fig. 3&4), we found that ethanol eliminated the differences in total neurite area (not significant; p = 0.98, Fig. 5A.d), GIRK2 puncta counts (p = 0.42, Fig. 5B.a), excitation following current injection (p = 0.32, Fig. 5E.a), step- (p = 0.48, Fig. 5E.b), and ramp- (p = 0.95, Fig. 5E.d) induced APs. Membrane capacitance was slightly but significantly reduced in the IEE AF group ($p = 9.6 \times 10^{-9}$, Fig. 5D.a). Other measurements were unchanged, again indicating that the cultured neurons exhibited similar differentiation properties. Results are consistent with the interpretation that neurite and excitability differences correlate with reduced GIRK2 expression, and that ethanol increases expression of GIRK2, potentially reversing these effects.

To confirm that both *KCNJ6* haplotype and ethanol exposure affect GIRK2 expression, we evaluated GIRK2 immunocytochemistry and *KCNJ6* mRNA in neurons using fluorescent in situ hybridization (FISH). GIRK2 increased following IEE ($p=1.3 \times 10^{-14}$, Fig. 5G-H). By probing *KCNJ6* fluorescent puncta colocalized with MAP2 immunocytochemistry, we confirmed that neurons from AF individuals had lower levels of *KCNJ6* mRNA expression compared to UN neurons (Fig. 5J.a, $p = 1.6 \times 10^{-3}$). We also found that the proportion of $MAP2^+$ neurons expressing KCNJ6 was reduced in AF compared with UN (50.1% vs 64.7%, Fig. 5J.b), and the AF neurons had a greater proportion of cells with low levels of expression (Fig. 5J.c) with no detectable High or Very High (>9 puncta/cell) expression. Differences in expression were found in somatic regions of neurons (Fig. 5J.f, $p = 4.1 \times 10^{-4}$) but not in non-somatic processes (Fig. 5J.g, p = 0.24). Ethanol increased *KCNJ6* mRNA levels in both groups (Fig. 5J.a-e), eliminating the difference between genotypes. Interestingly, we also observed that the proportions of AF neurons expressing KCNJ6 was increased (8.3%, Fig. 5J.b) by ethanol and was paralleled by a reduction in number of low-expressing cells and increased appearance of high-expressing neurons (Fig. 5J.c). Results indicate that variant *KCNJ6* haplotype leads to reduced *KCNJ6* expression, which is consistent with RNA

sequencing and immunocytochemical results, and that ethanol increases *KCNJ6* expression, eliminating differences between haplotype groups.

GIRK2 overexpression mimics IEE in human neurons with *KCNJ6* variants

To test if ethanol-induced GIRK2 expression could underlie the elimination of differences in neuronal properties associated with the *KCNJ6* haplotype, we compared ethanol treatment with virus transduced *KCNJ6* overexpression. Since ethanol has been shown to potentiate GIRK2-containing channels, we used a single treatment with 20 mM ethanol followed by fixation 24 h later. As expected, neither ethanol nor GIRK2 overexpression exhibited differences in passive neuronal properties. However, while current-induced activity increased in control cultures ($p = 6.8 \times 10^{-6}$, Fig. 6C), no significant difference was found in cultures exposed to 24 h ethanol ($p = 0.74$) and GIRK2 overexpression ($p = 0.23$). Similarly, while control cultures had increased ramp-induced APs ($p = 5.9 \times 10^{-4}$; Fig. 6A) neither GIRK overexpression ($p = 0.14$) or ethanol ($p = 0.10$) were significantly different. As a control, GIRK2 puncta count increased in a sample cell line after ethanol addition (line 376, $p = 0.04$, Fig. 6D) without an increase in circularity or solidity. These results indicate that the increased excitability in *KCNJ6* minor allele haplotype cells is due to reduced expression of GIRK2 protein and this effect is at least partially ameliorated or reversed by exposure to doses of ethanol found in human brain after moderate to heavy daily drinking.

Discussion

This study focused on the effect of an AUD- and endophenotype-linked *KCNJ6* haplotype on neuronal function, with a goal of identifying mechanisms that could eventually drive therapeutic strategies. To retain the appropriate genetic background for individuals with AUD, we selected subjects from the large NIAAA/COGA Sharing Repository, using both the selected *KCNJ6* haplotype and diagnosed alcohol dependence as criteria (Table 1). By preparing iPSC from these subjects and inducing them to model excitatory neurons, we identified differences in *KCNJ6* mRNA levels and GIRK2 immunoreactivity in individuals with variant *KCNJ6* haplotypes. Gene expression differences predicted effects on neuronal signaling including synaptic function. The *KCNJ6* haplotype was also associated with differences in the area of βIII-tubulin^{+} neuron projections and membrane excitability, but not in other measures of neuronal differentiation. Surprisingly, we found that ethanol exposure led to an increase in *KCNJ6* mRNA and GIRK2 expression, paralleled by a reduction or elimination of morphological and physiological differences in these neurons. Reversal of *KCNJ6* haplotype effects by ethanol could also be mimicked by overexpressing GIRK2. These results demonstrate that genetic variants enhancing risk of AUD, even if they do not alter protein sequence, can trigger neuronal mechanisms at the cellular level mirroring or predicting endophenotypes, here ERO, linked with AUD behavior.

Non-coding *KCNJ6* polymorphisms in AUD

Most GWAS SNPs map to non-coding regions of the genome and 3.7% are found in the UTRs (*39, 40*). The 3' UTRs of transcripts that are expressed in the brain tend to be longer than those expressed in other tissues and can be involved in post-transcriptional regulation of transcript abundance by affecting RNA stability, translation and/or localization (*41, 42*). Reference genome annotation of *KCNJ6* identifies two transcripts, one with a short 3' UTR (1,926 bp; Ensembl ENST00000645093, RefSeq NM_002240) and one with a substantially longer 3' UTR (18,112 bp; Ensembl ENST00000609713). RNAseq coverage analysis in human iN cultures detects only the longer isoform, although it is possible that a relatively small portion could be the shorter isoform, but the uniformly distributed coverage (Fig. 1B) does not indicate this. This longer transcript is orthologous to a 16-kb transcript found in rat brain (*43*), which includes multiple AU-rich elements, which may affect mRNA stability and could be affected by *KCNJ6* allelic variation. We conclude that the vast majority of *KCNJ6* mRNA is consistent with having the extended 3' UTR, with the potential for variant SNPs to affect mRNA stability or translation efficiency.

In addition to the three synonymous and intronic SNPs used to select subjects (Table 1), examination of variants in the long 3'UTR by RNAseq alignment predicts linkage of 19 additional SNPs (Fig. 1B; Supplemental Table 1). None of the 3' UTR SNPs could be mapped uniquely to known regulatory sequences such as predicted microRNA target sites. That is, some SNPs are predicted to destroy or add predicted targeting sites, but all of these sites were found in multiple locations within the 3' UTR, not only where they would be altered by a SNP. It is possible, however, that altered microRNA targeting of one or more sites among many in the 3'UTR could play a role in regulating the stability or translation of the variant *KCNJ6* mRNA, but no clear

candidates could be identified for testing. Furthermore, since ethanol exposure of neurons has been found to inhibit 1-carbon metabolic pathways, leading to selective changes in histone methylation (Sun et al., manuscript submitted), it remains possible that a sequence-specific epigenetic mechanism other than microRNAs may affect *KCNJ6* variant expression.

However, results demonstrate that the non-coding variant haplotype alters expression of GIRK2 protein and *KCNJ6* mRNA. We found that iN from subjects with the homozygous variant *KCNJ6* haplotype exhibited lower expression of GIRK2 by immunocytochemistry (Fig. 3D), but while the difference in neuronal mRNA levels as detected by scRNAseq analysis matched this trend, it did not reach significance ($p = 0.0508$; Fig. 1C). FISH analysis, however, confirmed that *KCNJ6* mRNA was reduced in the AF group (Fig. 5J). *KCNJ6* mRNA was also detected in fewer $MAP2^+$ cells and at lower levels per cell (Fig. 5J.b-c). The results of counting GIRK2 puncta and evaluating *KCNJ6* mRNA by scRNAseq and FISH support a diminished expression of GIRK2 in neurons from the affected group.

Surprisingly, ethanol exposure increased expression of both GIRK2 immunoreactivity and *KCNJ6* mRNA. Following 7 days of IEE with a peak concentration of 20 mM ethanol, GIRK2 puncta in the AF group increased to levels significantly higher than the UN group (Fig. 5B). Similarly, *KCNJ6* mRNA levels were shown to be increased above untreated levels by scRNAseq results (Fig. 1C) as well as FISH analysis (Fig. 5J). Ethanol also increased the proportion of $MAP2^+$ cells expressing *KCNJ6* as well as the expression level per cell (Fig. 5J.b-c). While previous studies identified a binding site for ethanol in a defined pocket of GIRK2 (*44*), suggesting that ethanol could affect protein stabilization, this binding could not explain the increased mRNA level. There is no indication that ethanol or *KCNJ6* haplotype altered translocation of *KCNJ6* mRNA to neuronal processes (Fig. 5J.d-e). Ethanol has been found to affect microRNA expression patterns that regulate mRNA (*41, 45-50*). It is intriguing to speculate that ethanol might increase expression of GIRK2 through this type of mechanism, with polymorphisms in the 3'UTR serving as the modulator.

GIRK2 in the context of alcohol dependence

GIRK channels play an essential role in maintaining the excitability of neurons. For example, in Trisomy 21 individuals, whose cells contain an additional copy of *KCNJ6*, neuronal activity was shown to be reduced due to excessive channel activity (*51-53*). On the other hand, loss of GIRK2 activity in knockout mice increases susceptibility to induced seizures (*20, 21*). We detected the presence of GIRK channel function in glutamatergic iNs using the ML297 agonist of GIRK1/2 heterotetramers, showing that activation led to a reduction in the frequency of action potentials induced by depolarization (Fig. 2D). However, only 6.7% of neurons responded to ML297, but overexpression of GIRK2 increased the proportion of responding neurons to 30% (Fig. 2D). We therefore chose to focus on evaluating neuronal excitability as an indirect response to changes in GIRK function.

By identifying the correlation between GIRK2 expression levels and altered GIRK2-mediated function, we predict that neuronal excitability will be affected by *KCNJ6* variants and alcohol

exposure. Human iNs generated from subjects with the variant *KCNJ6* haplotype and AUD were more excitable and had lower levels of GIRK2 expression. Moreover, ethanol exposure, both shorter (1 d) and longer (7 d) term, diminished these differences, mimicking the effect of GIRK2 overexpression. While GIRK channels play relatively small role in maintaining neuronal homeostasis, modulating GIRK activity to alter cell excitability is predicted to play a critical role. Additionally, downstream effectors of the G protein-mediated signaling pathways presumably regulate neuronal function indirectly (*14, 15, 17, 19*). GIRK channels are implicated in several other disorders with abnormal neuronal excitability, including epilepsy, suggesting that they have therapeutic potential (*19-21, 51-54*).

From genes to behavior

In this study, we found that the variant *KCNJ6* haplotype affects excitability of neurons (Fig. 3 & 4E). In Ca^{2+} imaging experiments, concomitant with enhanced excitability in neurons from affected individuals following stimulation with glutamate pulses, we observed an overall increase in basal activity of the neuronal population (Fig. 4F). This is reminiscent of the original observation linking *KCNJ6* variants with an EEG endophenotype, where Kamarajan and colleagues observed that individuals with alcohol dependence and the *KCNJ6* haplotype had an ERO theta power that varied as a function of the *KCNJ6* haplotype in both loss and gain conditions (*10*). There is an extensive human literature linking impulsivity to alcohol use problems (*55-58*). Impulsivity is elevated in offspring who are at high risk for substance use disorders and may be a reflection of a genetic vulnerability for substance use problems (*59*). Excitability in individual neurons and particularly in a culture dish of neurons is several levels of complexity removed from EEG patterns in brain. However, our study points to a mechanistic underpinning of how heritable risk traits are likely to play a role in development of unique physiological response to alcohol in the brain.

Materials and Methods

Generation of human iPS cells and glutamatergic neurons (iN)

Subjects were selected from the NIAAA/COGA Sharing Repository of the Collaborative Study on the Genetics of Alcoholism (COGA) project with characteristics summarized in Table 1. All subjects were of European ancestry. Cryopreserved lymphocytes were reprogrammed to iPSC using Sendai-viral-expressed transcription factors (Oct3/4, Sox2, Klf4 and c-Myc; Cytotune™-iPS Reprogramming Kit, ThermoFisher) by RUCDR Infinite Biologics® (now IBX, LLC.). Pluripotent cells were selected by colony morphology, alkaline phosphatase positivity, and immunocytochemical expression of Oct4 and TRA-1-60. Pluripotency was confirmed by colony morphology and immunocytochemistry for Oct4 and Tra-1-60 markers (Supplemental Fig. 1A). Identity of each iPSC line was confirmed by matching a 96 SNP panel to results obtained from fresh blood upon banking the original sample. Genomic integrity was confirmed using e-Karyotyping (*60*) using RNAseq data, which detected no anomalies (Supplemental Fig. 1B). Frozen aliquots were obtained for each subject, thawed, expanded, and maintained for neurogenesis. All iPS lines were cultured up to 50 passages for these experiments.

The previously-described protocol for generating glutamatergic human induced neurons (iN) (*61-63*) was modified. To obtain cultures with enhanced levels of spontaneous activity, we minimized the time of Ngn2 induction to reduce alternate cell identities (*27*) and fed cultures with a low-molality medium for at least 30 days post-induction (*64*). Briefly, iPS cells were plated as dissociated cells on Matrigel®Matrix (CorningLife Sciences)-coated dishes in iPS-Brew-XF (StemMACS) medium supplemented with 2 µM Y-27632 (Peprotech, Inc.) and 2 ng/µl doxycycline, and infected with lentiviruses expressing Ngn2 (AddGene #52047) and rtTA (FUW-M2rtTA; AddGene # 20342) for 10−12h. The next day, the culture medium was replaced with Neurobasal medium/B27/GlutaMAX™ (Life Technologies) supplemented with 2 µg/mL of doxycycline (MP Biomedical), 2 µM Y-27632 and 2 ng/µl puromycin. Puromycin selection was continued for 2 days, and on day 5, the induced neurons were dissociated with Accutase (STEMCELL Technologies) and plated on Matrigel-covered glass coverslips with a monolayer of primary astrocytes (passage 2-3) isolated from postnatal day 0-1 mouse pups, as described previously (*65*). Following plating, 50% of Neurobasal medium was changed to Neurobasal Plus culture medium with ascorbic acid, GlutaMAX, B27 Plus and Culture One supplements (Life Technologies). Half of the Neurobasal Plus medium with all supplements was replaced every 2−3 days. Cultures of iN typically exhibited resting membrane potentials averaging -40 mV with the presence of synaptic markers, spontaneous action potentials, and synaptic activity.

Intermittent Ethanol Exposure (IEE).

Since ethanol evaporates during culture incubation, we initially added ethanol to 20 mM and then replenished half the medium daily with 40 mM ethanol in medium. Ethanol concentrations were measured using and AM1 Alcohol Analyzer (Analox Instruments, Ltd.), as described previously (*25*).

Primary mouse cortical neuron cultures

P0-P1 mouse brains were obtained following decapitation on ice, meninges were removed, cortex was dissected and cells were dissociated by incubation in trypsin (Gibco) for 5-7 min at 37°C. The cells were then washed with Hank's balanced salt solution (HBS) and triturated by gentle pipetting. The cell suspension was centrifuged for 5 min at 160 x g and plated on Matrigel-coated glass coverslips in Neurobasal medium/B27/L-Glutamine (Life Technologies). When the density of glia in the culture reached ~40–50% (approximately 2 days after plating), 50% of the conditioned culture medium was replaced with fresh medium containing 4 mM Ara-C (Sigma; 2 mM final concentration). The cultures were maintained in medium containing 2 mM Ara-C until fixation at 13–18 days in vitro (DIV).

Generation of CRISPR/Cas9 Knockout iPSC

As a negative control for GIRK2 antibody validation we generated a *KCNJ6* knockout by CRISPR/Cas9 deletion. Two optimal gRNA targeting sequences were selected (using http://crispr.mit.edu) to generate a frameshift 76-bp deletion, introducing three termination codons within 40 bp following the deletion. A well-characterized iPSC line, WTB (*66*), was obtained from the Gladstone Institute Stem Cell Core Facility (San Francisco, CA). Approximately 3 x 10^6 WTB iPSC (passage 58) were electroporated (amaxa Nucleofector) in suspension with a mixture of two plasmids constructed from pSpCas9(BB)-T2A-GFP [AddGene #48138;(*67*)], with sequences targeting *KCNJ6*: G1, 5'-GATATCGGTCAGGTAGCGAT-3'; or G2, 5'-TCAGCCGAGATCGGACCAAA-3'. One day after transfection, cells were dissociated with Accutase and sorted to select GFP^+ cells into KSR medium (Life Technologies) with 2 µM Y-27632 and FGF (Peprotech, Inc.) and then plated at low density into two wells of a 6-well plate. Approximately 7-10 days later, individual colonies were hand-picked into 96-well plates. Three days after plating, cultures were split to two 96-well plates. One plate was harvested at ~50-100% confluence for screening. Cells were lysed in Quickextract (Lucigen), heated to 68°C for 6 minutes followed by 98°C for 2 minutes. The lysate was PCR amplified (DET3-F: 5'- TGGACCCCAACACAGATTGG-3' and -R: 5'- TGGATCAGGACGTCGAAAGC-3'), treated with exoSAPIT (Life Technologies) and analyzed by agarose gel electrophoresis. From 96 colonies, approximately 19 appeared to have a single-band deletion of the predicted size. Aliquots of the PCR reactions were sequenced with the F primer to confirm. To confirm homozygosity, PCR products from four candidates were cloned into a plasmid (StrataClone Blunt PCR Cloning Kit, Agilent) and individual colonies sequenced to identify each allele. Only one candidate, A7, exhibited the designed homozygous 76 bp deletion. A second colony with no deletion, E11, was selected to serve as unedited control.

Bulk and single cell RNA sequencing

For bulk RNAseq, individual iN cultures were harvested in lysis buffer and column purified (Quick-RNA kit, Zymo). Purified RNA was sent to Novogene, Inc., for sequencing. Fastq files were downloaded, filtered with Fastp (*68*), aligned to human reference genome (hg38) with HISAT2 (*69*), quantified with featureCounts() function from the Rsubread package (*70*), and analyzed with DESeq2 (*71*). These data have been deposited with the NIH GEO repository (accession number GSE196491).

For single-cell RNA sequencing (scRNAseq), iN cultures were treated with 20 mM ethanol for 7 days using an intermittent ethanol exposure (IEE) protocol where alcohol was replenished daily (*25*). At 28 days after plating onto glia, iN were dissociated using trypLE Express (Thermo Fisher) for 5 minutes at 37°C. The dissociated cells were centrifuged at 200 x g for 5 minutes at 4°C. The supernatant was removed, and cells were washed twice with 1X HBSS (Thermo Fisher). After washes, cells were resuspended in 1% BSA (Bovine Serum Albumen, ThermoFisher)/1xPBS (ThermoFisher). Cells were counted and resuspended at 1200 cells/µl in 1% BSA/ 1xPBS and placed on ice. Single-cell cDNA libraries were generated using the Chromium Next GEM Single Cell 3' GEM Reagent Kits v3.1 (10X Genomics). Approximately 20,000 dissociated cells were loaded onto a cassette in the Chromium Controller with accompanying reagents to generate Gel Beads in Emulsions (GEMs). GEMs were subjected to reverse transcription to generate single-cell cDNA libraries before the oil emulsion was disrupted and cDNA purified using Dynabeads MyOne Silane (Thermo Fisher). cDNA was amplified by PCR for 11 cycles and purified using SPRIselect reagent (Beckman Coulter). cDNA fragmentation, A-tailing, and end repair was performed followed by adapter ligation for paired-end sequencing. An additional 11 cycles of PCR were performed to incorporate the sample index sequences and to amplify the libraries before samples were purified using SPRIselect reagent and used for sequencing. Libraries were shipped to Psomagen, Inc., for sequencing service. Fastq files were downloaded, aligned with reference genome (initially hg38 and mm10) using CellRanger (10XGenomics) and then imported into Seurat (*72*) for processing. Summary data are listed in Supplemental Figure 3. These data have been deposited with the NIH GEO archive, accession number GSE203530.

Fluorescent in situ hybridization (FISH)

Fluorescent, single molecule *in situ* hybridization was performed with the RNAscope® Multiplex Fluorescent Detection Kit v2 (Advanced Cell Diagnostics, ACD) following the manufacturer's instructions. In brief, iN cultures were fixed in 4% paraformaldehyde for 20 min at room temperature, followed by a series of ethanol dehydration/rehydration steps, permeabilization (with PBS-0.01% Tween buffer), blocking and overnight incubation with primary antibody against MAP2 (Millipore AB5543, 1:100 dilution). Prior to probe hybridization, samples were treated with hydrogen peroxide for 10 min and then with protease III (1:10) for 10 min. Human-specific *KCNJ6* probe was hybridized for 2 h, followed by standard amplification and color reaction with 520 Opal dye (Akoya Biosciences). MAP2 antibody was labeled with secondary antibody (Alexa 633), nuclei were stained with DAPI, and coverslips were mounted on slides using mounting medium (Thermo Fisher). Images were acquired on a Zeiss LSM 800 confocal microscope using a 40x objective. *KCNJ6* was quantified by manually counting fluorescent puncta within the MAP2/DAPI positive regions of individual neurons (defined as "somatic") or as puncta scattered along the MAP2-associated processes ("non-somatic"). Levels of *KCNJ6* were binned according to semi-quantitative histological scoring methodology by levels using Advanced Cell Diagnostics scoring criteria, where low expression of RNA target was defined to be 1-3 puncta per cell, intermediate 4-9, high 10-15 and very high >15 per cell.

Electrophysiology

Functional analyses of induced human neurons were performed using whole-cell patch-clamp electrophysiology as previously described (*24, 25*). Recordings were done in HEPES buffer consisting of (in mM): 140 NaCl, 5 KCl, 2 $CaCl_2$, 2 $MgCl_2$, 10 HEPES, 10 Glucose. Osmolality of the buffer was between 290-305 mOsm and the pH was adjusted to 7.4. Whole-cell patch-clamp recordings were performed using borosilicate glass electrodes with resistances of 4-8 MΩ and intracellular solution containing the following (in mM): 126 K-Gluconate, 4 KCl, 10 HEPES, 4 ATP-Mg, 0.3 GTP-Na_2, 10 Phosphocreatine, with pH adjusted to 7.2 and osmolarity to 270−290 mOsm. After patching, neurons were allowed to rest for 5-7 min, or until the RMP drift stabilized, before recording. For GIRK2 channel recordings, an extracellular solution with high K^+ was used, which consisted of: 20 mM KCl, 140 mM NaCl, 2 mM $CaCl_2$, 2 mM $MgCl_2$ and 10 mM HEPES (pH 7.4). GIRK-mediated currents were measured at -40 mV membrane potential holding. Excitability of the neurons was measured by applying ramp (+200 pA) and step (-50 pA – 100 pA) depolarizing pulses while holding neurons at -65mV (current clamp mode). All recordings in cultured human neurons were performed at room temperature. Cells were excluded from analysis if access resistance changed by more than 20% across the duration of the recording. For current injection studies, neurons were excluded if RMP was close to -63mV and the required current injection was less than 1 pA (absolute value). In addition, any induced neurons whose access resistance was greater than 35 MΩ were also excluded. Drugs were applied through a perfusion system in the following concentrations: 160 nM ML297 or 20 mM alcohol. Clampfit software (pClamp 11; Molecular Devices) was used for analysis of recordings.

Immunocytochemistry and confocal imaging

iN cultures were fixed for 30 min in ice cold methanol and permeabilized using 0.2% Triton X-100 in PBS for 15 min at room temperature. Cells were then incubated in blocking buffer (5% BSA with 5% normal goat serum in PBS) for 30 min at room temperature and then incubated with primary antibodies diluted in blocking buffer overnight at 4°C, washed with PBS three times, and subsequently incubated with secondary antibodies for 1 h at room temperature. Confocal imaging analysis was performed using a Zeiss LSM700. Primary antibodies used: rabbit anti-GIRK2 (Alomone labs, APC-006, 1:400), mouse anti-βIII-tub (Bio legend, MMS-435P,1:1000), chicken anti-MAP2 (Millipore AB5543, 1:1000), mouse anti-Syn1 (SYSY,106-011, 1:200), mouse anti-PSD 95 (SYSY, 124-011, 1:2000), mouse anti-mCherry (Thermofisher Scientific, M11217, 1:100).

Validation of GIRK2 immunoreactivity

To validate the specificity of GIRK2 detection, GIRK2 was overexpressed by transduction with a ubiquitin C (UbiC) promoter-driven, *KCNJ6*-expressing lentivirus or expression was eliminated by introducing frameshift deletions into *KCNJ6* using CRISPR/Cas9-editing. Overexpression was initiated by infection on day 27 post-induction and GIRK2 expression was evaluated 14 days later. Levels of GIRK2 in iN prepared from the CRISPR/Cas9 knockout line were measured at a similar time post-induction (~day 40). Viral GIRK2 transduction was confirmed by co-expression of mCherry.

Image analysis

Cytometric analysis of confocal images of MAP2-stained iN cultures was performed using the Fiji/ImageJ image analysis program (*73*). Regions of Interest (ROIs) were created for each cell by encapsulating the cell body through use of the cell magic wand tool. The cell body was then quantified for area and shape descriptors. The NeurphologyJ Fiji macro (*74*) was utilized for detection and quantification of extended neuronal morphometry. A threshold was selected manually so that most neurites are well-defined without significant particle detection or noise. GIRK2 puncta quantification used trainable Weka Segmentation (*75*) to segment the image to establish two classes. One class identified pixels that corresponded to GIRK2 puncta for intensity, circularity, and size. A second class identified pixels that did not correspond to puncta, such as noise from neurons and background. The classifier was trained multiple times until there was a high confidence that the pixels segmented into class one had a high (90%) confidence interval denoted by probability maps. The segmented image was adjusted to remove any false negatives. The class one binary image was then used for puncta cytometry.

Lentiviruses

FSW-hSyn-GCaMP6f assembly was described previously (*76*). FUGW-KCNJ6-mCherry was assembled using lentiviral backbone from FUGW (AddGene #14883), *KCNJ6* coding sequence amplified from human neuron cDNA (forward primer: agccaggaaaagcacaaaga, reverse primer: ggggagaagagaagggtttg), and mCherry with a nuclear localization signal from pME-nlsmCherry (a gift from Dr. Kelvin Kwan). During construction, the GIRK2 protein-coding sequence was tagged with a 3xHA tag and linked to mCherry with a T2A “self-cleaving” element.

Calcium imaging in iPSC-derived iN populations

For assessing neuronal excitability, iN co-cultured with mouse glia on Matrigel™ coated 10 mm glass coverslips were transduced with lentivirus expressing hSyn-GCaMP6f at least 2 weeks prior to imaging to ensure robust expression. All fluorescence imaging experiments were performed in ~50 DIV (days in vitro) iNs. Coverslips were mounted on a diamond-shaped chamber and placed on a Nikon Eclipse TE2000-U microscope with a 10X objective. GCaMP6f was excited using a 480 nm (Mic-LED-480A, Prizmatix), a HQ480/40x excitation filter, a Q505LP dichroic mirror, and a HQ535/50m emission filter (Semrock). Fluorescence was projected onto a sCMOS Zyla 5.5 camera (Andor) and sampled at a rate of 4.7 fps with a frame exposure of 200 ms at 160x120 pixels (4x4 binning). Light source and sCMOS camera were controlled with the Nikon Elements software (NIS-Elements AR 5.20.01).

Neurons were continuously perfused during fluorescence recording with ACSF with the following composition (in mM): NaCl 125, KCl 5, D-Glucose 10, HEPES-Na 10, $CaCl_2$ 3.1 and $MgCl_2$ 1.3. The pH was adjusted to 7.4 with HCl and osmolarity corrected with sucrose to 290-300 mOsm. Depolarizing solutions were prepared in ACSF with 10 or 50 µM glutamate, or with 18 mM KCl. Perfusion was gravity fed (flow rate of 0.065 ml/s). Solution exchanges were controlled with a ValveBank8 II (AutoMate Scientific Inc.). Calcium transients were recorded using a protocol based on glutamate and KCl perfusion, that consisted of 3 min baseline activity (ACSF), 3 x 30 s pulses

of 10 µM glutamate (30 s ACSF between pulses), one 30 s pulse of 50 µM glutamate, 2 min of ACSF wash, 3 x 30 s pulses of 18 mM KCl (30 s ACSF between pulses), and a final ACSF wash for 5 min (Fig. 4C).

ROI segmentation of GCaMP6f-expressing neurons, raw fluorescence extraction and background correction were performed with Nikon Elements software. ΔF/F was calculated with the formula $(F_t - F_{min})/F_{min}$, where F_t is the raw fluorescence at time t and F_{min} is the minimum fluorescence for the entire trace. The resulting trace was then denoised with a low-pass Butterworth filter and baseline corrected for drift using an adaptative iteratively reweighted Penalized Least Squares (AirPLS) based algorithm (*77*), in R-studio (R version 4.0.3). Peak detection was performed using a custom script in R that considered neuron action potential-derived Ca^{2+} spikes that had the following criteria (for a framerate acquisition of 4.7 fps): duration < 30 frames, rise phase >= 2 frames, fall phase >= 5 frames, rise phase < fall phase, peak height > 5*SD, and peak height > 5*max background signal. The analysis pipeline is depicted in Supp. Fig. 7. Statistical analysis was performed in GraphPad Prism 8.4.3 or R version 4.0.3.

Statistics

Parameters that were sampled in cells from multiple microscopic fields and from multiple cell lines were fit to a linear mixed-effects model using the lme4 package in R (*78*). The model included the cell line identifier and sex. A Tukey post-hoc test identified pairwise differences in two-factor models (e.g., combined genotype and ethanol exposure). Electrophysiology results were modeled using generalized estimating equations (GEE) with the cell line as grouping identifier using the geepack R package (*79*). Where appropriate, ANOVA or t-test was used as indicated in figure legends. For RNAseq, pseudo-bulk data (single cell reads pooled by subject identifier) were modeled in DESeq2 (*71*), testing first by likelihood ratio testing (LRT) over all groups, and then pairwise comparisons were evaluated using Wald tests. After Benjamini-Hochberg multiple measurements correction, a false discovery rate of 5% was set as a threshold for significance.

Acknowledgements

The Collaborative Study on the Genetics of Alcoholism (COGA), Principal Investigators B. Porjesz, V. Hesselbrock, T. Foroud; Scientific Director, A. Agrawal; Translational Director, D. Dick, includes eleven different centers: University of Connecticut (V. Hesselbrock); Indiana University (H.J. Edenberg, T. Foroud, Y. Liu, M. Plawecki); University of Iowa Carver College of Medicine (S. Kuperman, J. Kramer); SUNY Downstate Health Sciences University (B. Porjesz, J. Meyers, C. Kamarajan, A. Pandey); Washington University in St. Louis (L. Bierut, J. Rice, K. Bucholz, A. Agrawal); University of California at San Diego (M. Schuckit); Rutgers University (J. Tischfield, R. Hart, J. Salvatore); The Children's Hospital of Philadelphia, University of Pennsylvania (L. Almasy); Virginia Commonwealth University (D. Dick); Icahn School of Medicine at Mount Sinai (A. Goate, P. Slesinger); and Howard University (D. Scott). Other COGA collaborators include: L. Bauer (University of Connecticut); J. Nurnberger Jr., L. Wetherill, X., Xuei, D. Lai, S. O'Connor, (Indiana University); G. Chan (University of Iowa; University of Connecticut); D.B. Chorlian, J. Zhang, P. Barr, S. Kinreich, G. Pandey (SUNY Downstate); N. Mullins (Icahn School of Medicine at Mount Sinai); A. Anokhin, S. Hartz, E. Johnson, V. McCutcheon, S. Saccone (Washington University); J. Moore, Z. Pang, S. Kuo (Rutgers University); A. Merikangas (The Children's Hospital of Philadelphia and University of Pennsylvania); F. Aliev (Virginia Commonwealth University); H. Chin and A. Parsian are the NIAAA Staff Collaborators. We continue to be inspired by our memories of Henri Begleiter and Theodore Reich, founding PI and Co-PI of COGA, and also owe a debt of gratitude to other past organizers of COGA, including Ting- Kai Li, P. Michael Conneally, Raymond Crowe, and Wendy Reich, for their critical contributions. This national collaborative study is supported by NIH Grant U10AA008401 from the National Institute on Alcohol Abuse and Alcoholism (NIAAA) and the National Institute on Drug Abuse (NIDA).

Supplementary Materials

Supplementary Tables 1-4: https://doi.org/10.6084/m9.figshare.19798882.v1

Supplemental Table 1. SNPs identified in RNAseq samples. Variants were identified in the region surrounding KCNJ6 (chr21: 37499112-38245792) using samtools mpileup to bcftools call, followed by filtering to remove low quality. Results were loaded into the Ensembl VEP tool. A dot (".") indicates missing data and/or low quality. The reference allele and alternate alleles were obtained from the UCSC Genome Table Browser.

Supplemental Table 2. Differentially expressed genes (DEG) comparing AF to UN without exposure to ethanol. The table contains all output from DESeq2 results. Excel filters are set to show only genes significantly different (padj <= 0.05) and at least 1.5-fold different (abs(log2FoldChange) > 0.585). Release the filters to see the full list.

Supplemental Table 3. Enriched Gene Ontology-Biological Process (GO-BP) terms from genes increased in AF relative to UN.

Supplemental Table 4. Enriched Gene Ontology-Biological Process (GO-BP) terms from genes decreased in AF relative to UN.

Supplementary Figures and Methods: https://doi.org/10.6084/m9.figshare.19798873.v1

Figure Legends

Figure 1. Experimental design and gene expression analysis

A. Diagram outlining experimental design. Lymphocytes from subjects with or without AUD diagnosis and *KCNJ6* haplotype variants were selected, reprogrammed into iPSC, induced into excitatory iNs, and analyzed by morphometry, immunocytochemistry, gene expression, and electrophysiology. **B.** Sequencing alignment and depth analysis of bulk RNA sequencing confirmed expression of *KCNJ6* mRNA in iN cultures, specifically the ENST00000609713 isoform, containing an 18.1 kilobase 3'UTR region. Depth: number of sequencing reads per base aligned by position. Frequency: thickness of curved lines represents the relative frequency of splice site utilization between exons. Variant analysis of RNA sequences predicts a region of linkage disequilibrium of 22 SNPs, including the 3 SNPs used to select subjects (red, Table 1), and 19 additional SNPs (blue, Supplemental Table 1). **C.** Single-cell RNAseq identifies a cluster of induced neurons (upper right), expressing markers consistent with neuronal function including *SYP*, *SCN3A*, *SLC17A6*, *GRIN2B*, *KCNJ3*, and *KCNJ6*; distinct from "transition neurons" that either do not express these markers or express sporadically. Isolating *KCNJ6* mRNA expression, aggregated by subject and treatment, AF neurons expressed a trend towards lower levels than UN neurons ($p = 0.0508$; Wald test), but treatment of 7d with IEE at 20 mM peak concentration increased AF expression above untreated ($p = 0.0225$) to levels similar to UN control ($p = 0.322$, not denoted on figure). **D.** Volcano plot for untreated UN vs AF neurons, highlighting genes significantly different (FDR > 0.05) and at least 1.5-fold changed (red dots). Genes below the fold-change cut-off are marked in green, and those not significantly different are marked in blue. Significantly different genes are listed in Supplemental Table 2. **F.** Gene ontology (GO) enrichment of top 10 biological process (BP) terms for up- or down-regulated genes. Plots indicate the number of regulated genes from the term and the color indicates the adjusted p-value (q-value; key). All enriched terms are listed in Supplemental Table 3.

Figure 2. Validation of GIRK2 expression and function in human induced neurons.

A. Representative confocal images of GIRK2 immunoreactivity in mouse cortical neurons. Arrowheads indicate locations of GIRK2-staining puncta, with an example punctum enlarged in the inset, overlapping or adjacent to βIII-tubulin-positive processes. We observed two cellular expression patterns – one where the entire neuron is decorated with GIRK2 antibody (Supplemental Fig. 5), or another where GIRK2 expression is relatively faint and observed mostly on neuronal processes, shown here. **B**. GIRK2 expression patterns in human induced neurons (iNs), showing representative confocal images from line 420. Inset shows two adjacent puncta. **C**. Following infection of iN cultures with lentivirus expressing *KCNJ6* and mCherry, large numbers of GIRK2$^+$ puncta are seen in representative images (line 420). **D**. Evaluation of GIRK2 function in iNs, (a) quantification of GIRK2 expression on MAP2$^+$ vs. βIII-tubulin$^+$ neuronal processes. GIRK2 is more abundant on βIII-tubulin processes ($p=0.014$). (b) Basal levels (upper pie plot) of the GIRK current in iNs as percent of neurons responding with hyperpolarization to the selective GIRK activator (160 nM ML297); compared with responding percentage when

GIRK2 is overexpressed (lower pie chart). (c) Representative image of iN overexpressing GIRK2, as confirmed with mCherry fluorescence. (d) Representative traces of induced action potential firing before and after GIRK activation, demonstrating the contribution of GIRK function to cell excitability. (e) Representative trace of spontaneous postsynaptic potential (sEPSCs) recordings during ML297 (160 nM) GIRK activator wash-in, demonstrating a shift of 7mV holding current (amplifier-dependent compensation of GIRK-mediated membrane hyperpolarization). (f) Quantification of neuronal excitability at baseline and following GIRK activation with ML297 (160 nM). Student's t-test was used to evaluate differences (*p < 0.05, **p < 0.01).

Figure 3. Impact of AUD-associated *KCNJ6* haplotype on neuronal properties.
A. Principles of morphological analysis of induced neurons: (a) Neurite area was the total TuJ1$^+$ (βIII-tubulin)$^+$ staining area outside the cell soma. (b) Solidity is the area of the soma divided by its convex hull area. (c) Soma size was the area of the MAP2$^+$ cell body. (d) Circularity compared the perimeter to the area. **B**. Morphometry of iNs from *KCNJ6* haplotype variant and affected (**AF**, cyan) or unaffected (**UN**, grey) individuals. Results are summed by group (left) or plotted individually by cell line (right), with subjects identified by line number (see Table 1--females identified with grey numbers). Individual cells are plotted as dots with the bar showing the mean, with bars indicating the standard error of the mean (SEM). No significant differences were found in (a) soma size, (b) circularity, or (c) soma solidity, but total neurite area was increased in the AF group (p = 0.0007). **C**. Representative images of iNs from individual lines, with arrows identifying individual GIRK2 puncta (red) localized on βIII-tubulin$^+$ processes (gray). **D**. GIRK2 expression was decreased in the AF as measured by puncta counts (a, p = 0.043), while there was no difference in puncta size (b), circularity (c), or solidity (d). **E**. Representative images of individual GIRK2 puncta (red) localized on βIII-tubulin$^+$ processes (gray). **F**. Electrophysiological analysis of passive neuronal properties, showing no difference in (a) membrane capacitance (b) membrane resistance, or (c) spontaneous EPSCs frequency. (d) Representative sEPSCs traces for each line. (e) Spontaneous EPSCs amplitude. **G**. Electrophysiological analysis of active neuronal properties. (a) Quantification of current required to shift resting membrane potential to -65mV in pA: difference by group p = 0.048; (b) quantification of maximum number of action potentials (APs) induced with the "step" protocol, p = 0.014; (c) representative traces of APs induced with the "step" protocol; (d) quantification of number of action potentials (APs) induced with the "ramp" protocol, p = 0.036; (e) representative traces of APs induced with the "ramp" protocol. A generalized linear model was used to evaluate group differences for morphometry and GIRK2 expression, and generalized estimation equations was used for electrophysiology results (*p < 0.05, **p < 0.01, ***p < 0.001).

Figure 4. Evaluation of neuronal excitability in human induced neuron populations.
A. Representative epifluorescence images of GCaMP6f expression in iNs from affected (233, 246) and unaffected individuals (420, 472). **B, C.** Raster plots of the calcium spiking pattern of representative experiments from unaffected neurons (**B**, individual 472) and affected neurons (**C**, individual 233), under the stimulation protocol used. Green and purple bars show the

application of 30 s pulses of Glu 10-50 µM and KCl 18 mM, respectively, on the neuron populations during the stimulation protocol. Arrows show the epochs of the calcium imaging recordings selected for calcium spike quantification: baseline, glutamate pulse 1, and KCl pulse 1. **D.** Stimulation protocol (upper bar) and representative raw fluorescence trace (AF individual 233) from a complete recording. The zoom-ins on the first glutamate and KCl pulses depict glutamate and KCl elicited activity, respectively. The vertical dotted lines correspond to the calcium spikes detected after analysis. **E, F, G.** Number of spikes per ROI per minute during baseline (**E**, spontaneous activity), glutamate pulse 1 (**F**, glutamate-elicited activity) and KCl pulse 1 (**G**, KCl-elicited activity). The pie charts represent the proportion of neurons of UN (grey) and AF (blue) individuals that exhibited a certain number of calcium spikes during each three epochs of the recording. The bar plots show the number of spikes per ROI per minute fired by unaffected individuals (grey) and affected individuals (blue) during baseline, glutamate pulse 1 and KCl pulse 1. The sample size is depicted in the bar of each group as number of iN batches/number of experiments/number of neurons. Differences between affected and unaffected groups were evaluated by two-tailed unpaired Student's t-test (Welch's correction for non-equal SD, **p < 0.01, ****p < 0.0001).

Figure 5. Ethanol treatment reduced *KCNJ6* haplotype differences in iN excitability and GIRK2 expression.

A. Morphological analysis of IEE iNs generated from affected and unaffected individuals, showing no difference in: (a) neuronal soma size (p = 0.38); (b) soma circularity (p = 0.47); (c) soma solidity (p = 0.87); and (d) total neurite area (p = 0.98). **B**. There was no difference in GIRK2 expression in the IEE AF group iNs compared with UN by (a) puncta counts (p = 0.28), (b) puncta size (p = 0.34), or (d) solidity (p = 0.43), but there was a slight increase in (c) puncta circularity (p = 0.046). **C**. Representative images of individual GIRK2 puncta (red) localized on βIII-Tubulin positive processes (gray) for each cell line. **D**. Electrophysiological analysis of passive neuronal properties in IEE iNs, showing (a) a small decrease in AF membrane capacitance ($p = 9.6 \times 10^{-9}$), but no difference in (b) membrane resistance (p = 0.63), (c) spontaneous EPSCs frequency (p = 0.32), or (d) spontaneous EPSCs amplitude (p = 0.19). (d) Representative sEPSCs traces for each cell line. (f) The AF group exhibited no change in resting membrane potential after IEE (p = 0.79). **E**. Electrophysiological analysis of active neuronal properties found no difference in IEE iNs for (a) current required to shift resting membrane potential to -65mV (p = 0.32), (b) maximum number of action potentials (APs) induced with the "step" protocol (p = 0.48), with (c) representative traces of APs induced with the "step" protocol, (d) number of action potentials (APs) induced with the "ramp" protocol (p = 0.95), with (e) representative traces of APs induced with the "ramp" protocol. **F**. Representative images from individual lines of iNs, marked with arrows pointing to individual GIRK2 puncta (red) localized on βIII-Tubulin positive processes (gray). **G**. Summarized results from all lines showing differences in GIRK2 expression levels before and after 7 days of 20 mM IEE with ethanol (EtOH). **H.** Representative images of individual GIRK2 puncta (red) localized on βIII-Tubulin positive processes (gray) prior and following 7 days 20 mM IEE with ethanol. **I.**

Representative images of FISH detection of *KCNJ6* mRNA for each cell line. **J.** Quantification of FISH. (a) The number of *KCNJ6* puncta normalized to the number of cells in an image shows decreased expression in control AF compared with UN ($p = 1.6 \times 10^{-3}$), increased expression following IEE ($p = 1.1 \times 10^{-3}$; Tukey's pairwise comparisons for UN $p = 9.0 \times 10^{-3}$, for AF $p = 5.5 \times 10^{-3}$). (b) The percentage of *KCNJ6*-expressing $MAP2^{+}$ cells substantially increase in the (c) AF group but not in the (b) UN group. Numbers of *KCNJ6* puncta were analyzed by expression levels per cell, as recommended by the FISH manufacturer in (d) UN or (e) AF cells. (f) *KCNJ6* puncta within the neuronal soma show increases following IEE in both UN and AF groups ($p = 4.1 \times 10^{-4}$, Tukey's post-hoc for UN, $p = 1.1 \times 10^{-3}$, for AF, $p = 1.1 \times 10^{-3}$). (g) A similar analysis of non-somatic puncta, presumably within neurites, showed no differences following IEE (p=0.24).

Figure 6. GIRK2 overexpression mimics ethanol response

A. Current required to shift resting membrane potential to -65mV, in untreated (control, $p = 5.9 \times 10^{-4}$), lentiviral *KCNJ6* overexpression (over., p = 0.23), or 1 d 20 mM IEE (EtOH, p = 0.75) cultures. **B.** Representative traces of APs induced with the "ramp" protocol. **C.** Quantification of maximum number of action potentials (APs) induced with "ramp" protocol, control ($p = 6.8 \times 10^{-6}$), overexpression (p = 0.014), or 1 d 20 mM IEE (p = 0.10). **D.** quantification of GIRK2 puncta after overexpression (line 376, one-sided t-test p = 0.04).

References

1. B. Verhulst, M. C. Neale, K. S. Kendler, The heritability of alcohol use disorders: a meta-analysis of twin and adoption studies. *Psychol Med* **45**, 1061-1072 (2015).
2. M. S. Pollard, J. S. Tucker, H. D. Green, Jr, Changes in Adult Alcohol Use and Consequences During the COVID-19 Pandemic in the US. *JAMA Network Open* **3**, e2022942-e2022942 (2020).
3. C. Bouza, M. Angeles, A. Muñoz, J. M. Amate, Efficacy and safety of naltrexone and acamprosate in the treatment of alcohol dependence: a systematic review. *Addiction* **99**, 811-828 (2004).
4. M. Heilig, M. Egli, Pharmacological treatment of alcohol dependence: Target symptoms and target mechanisms. *Pharmacology & Therapeutics* **111**, 855-876 (2006).
5. M. D. Skinner, P. Lahmek, H. Pham, H. J. Aubin, Disulfiram efficacy in the treatment of alcohol dependence: a meta-analysis. *PLoS One* **9**, e87366 (2014).
6. J. E. Salvatore, Gottesman, II, D. M. Dick, Endophenotypes for Alcohol Use Disorder: An Update on the Field. *Curr Addict Rep* **2**, 76-90 (2015).
7. D. B. Chorlian, M. Rangaswamy, N. Manz, J. L. Meyers, S. J. Kang, C. Kamarajan, A. K. Pandey, J. C. Wang, L. Wetherill, H. Edenberg, B. Porjesz, Genetic correlates of the development of theta event related oscillations in adolescents and young adults. *Int J Psychophysiol* **115**, 24-39 (2017).
8. S. J. Kang, M. Rangaswamy, N. Manz, J. C. Wang, L. Wetherill, T. Hinrichs, L. Almasy, A. Brooks, D. B. Chorlian, D. Dick, V. Hesselbrock, J. Kramer, S. Kuperman, J. Nurnberger, Jr., J. Rice, M. Schuckit, J. Tischfield, L. J. Bierut, H. J. Edenberg, A. Goate, T. Foroud, B. Porjesz, Family-based genome-wide association study of frontal θ oscillations identifies potassium channel gene KCNJ6. *Genes Brain Behav* **11**, 712-719 (2012).
9. T. K. Clarke, M. Laucht, M. Ridinger, N. Wodarz, M. Rietschel, W. Maier, M. Lathrop, A. Lourdusamy, U. S. Zimmermann, S. Desrivieres, G. Schumann, KCNJ6 is associated with adult alcohol dependence and involved in gene × early life stress interactions in adolescent alcohol drinking. *Neuropsychopharmacology* **36**, 1142-1148 (2011).
10. C. Kamarajan, A. K. Pandey, D. B. Chorlian, N. Manz, A. T. Stimus, H. J. Edenberg, L. Wetherill, M. Schuckit, J. C. Wang, S. Kuperman, J. Kramer, J. A. Tischfield, B. Porjesz, A KCNJ6 gene polymorphism modulates theta oscillations during reward processing. *Int J Psychophysiol* **115**, 13-23 (2017).
11. C. Andrew, G. Fein, Event-related oscillations versus event-related potentials in a P300 task as biomarkers for alcoholism. *Alcohol Clin Exp Res* **34**, 669-680 (2010).
12. C. Kamarajan, M. Rangaswamy, Y. Tang, D. B. Chorlian, A. K. Pandey, B. N. Roopesh, N. Manz, R. Saunders, A. T. Stimus, B. Porjesz, Dysfunctional reward processing in male alcoholics: an ERP study during a gambling task. *J Psychiatr Res* **44**, 576-590 (2010).
13. I. W. Glaaser, P. A. Slesinger, Structural Insights into GIRK Channel Function. *International review of neurobiology* **123**, 117-160 (2015).
14. C. Luscher, P. A. Slesinger, Emerging roles for G protein-gated inwardly rectifying potassium (GIRK) channels in health and disease. *Nat Rev Neurosci* **11**, 301-315 (2010).
15. Y. Zhao, I. Gameiro-Ros, I. W. Glaaser, P. A. Slesinger, Advances in Targeting GIRK Channels in Disease. *Trends Pharmacol Sci* **42**, 203-215 (2021).
16. E. Reuveny, P. A. Slesinger, J. Inglese, J. M. Morales, J. A. Iñiguez-Lluhi, R. J. Lefkowitz, H. R. Bourne, Y. N. Jan, L. Y. Jan, Activation of the cloned muscarinic potassium channel by G protein beta gamma subunits. *Nature* **370**, 143-146 (1994).

17. P. Aryal, H. Dvir, S. Choe, P. A. Slesinger, A discrete alcohol pocket involved in GIRK channel activation. *Nat Neurosci* **12**, 988-995 (2009).
18. K. Bodhinathan, P. A. Slesinger, Alcohol modulation of G-protein-gated inwardly rectifying potassium channels: from binding to therapeutics. *Front Physiol* **5**, 76 (2014).
19. Y. A. Blednov, M. Stoffel, S. R. Chang, R. A. Harris, Potassium channels as targets for ethanol: studies of G-protein-coupled inwardly rectifying potassium channel 2 (GIRK2) null mutant mice. *J Pharmacol Exp Ther* **298**, 521-530 (2001).
20. Y. A. Blednov, M. Stoffel, S. R. Chang, R. A. Harris, GIRK2 deficient mice. Evidence for hyperactivity and reduced anxiety. *Physiol Behav* **74**, 109-117 (2001).
21. K. G. Hill, H. Alva, Y. A. Blednov, C. L. Cunningham, Reduced ethanol-induced conditioned taste aversion and conditioned place preference in GIRK2 null mutant mice. *Psychopharmacology (Berl)* **169**, 108-114 (2003).
22. R. Lieberman, E. S. Levine, H. R. Kranzler, C. Abreu, J. Covault, Pilot study of iPS-derived neural cells to examine biologic effects of alcohol on human neurons in vitro. *Alcohol Clin Exp Res* **36**, 1678-1687 (2012).
23. R. Lieberman, H. R. Kranzler, E. S. Levine, J. Covault, Examining the effects of alcohol on GABA(A) receptor mRNA expression and function in neural cultures generated from control and alcohol dependent donor induced pluripotent stem cells. *Alcohol* **66**, 45-53 (2018).
24. A. Halikere, D. Popova, M. S. Scarnati, A. Hamod, M. R. Swerdel, J. C. Moore, J. A. Tischfield, R. P. Hart, Z. P. Pang, Addiction associated N40D mu-opioid receptor variant modulates synaptic function in human neurons. *Mol Psychiatry* **25**, 1406-1419 (2020).
25. M. S. Scarnati, A. J. Boreland, M. Joel, R. P. Hart, Z. P. Pang, Differential sensitivity of human neurons carrying mu opioid receptor (MOR) N40D variants in response to ethanol. *Alcohol* **87**, 97-109 (2020).
26. C. Patzke, J. Dai, M. M. Brockmann, Z. Sun, P. Fenske, C. Rosenmund, T. C. Südhof, Cannabinoid receptor activation acutely increases synaptic vesicle numbers by activating synapsins in human synapses. *Mol Psychiatry*, (2021).
27. H. C. Lin, Z. He, S. Ebert, M. Schörnig, M. Santel, M. T. Nikolova, A. Weigert, W. Hevers, N. N. Kasri, E. Taverna, J. G. Camp, B. Treutlein, NGN2 induces diverse neuron types from human pluripotency. *Stem Cell Reports* **16**, 2118-2127 (2021).
28. J. M. Mitchell, J. Nemesh, S. Ghosh, R. E. Handsaker, C. J. Mello, D. Meyer, K. Raghunathan, H. de Rivera, M. Tegtmeyer, D. Hawes, A. Neumann, R. Nehme, K. Eggan, S. A. McCarroll, Mapping genetic effects on cellular phenotypes with “cell villages”. *bioRxiv*, 2020.2006.2029.174383 (2020).
29. F. Lesage, E. Guillemare, M. Fink, F. Duprat, C. Heurteaux, M. Fosset, G. Romey, J. Barhanin, M. Lazdunski, Molecular properties of neuronal G-protein-activated inwardly rectifying K+ channels. *J Biol Chem* **270**, 28660-28667 (1995).
30. C. E. Ang, M. Wernig, Induced neuronal reprogramming. *J Comp Neurol* **522**, 2877-2886 (2014).
31. H. Shelby, T. Shelby, M. Wernig, Somatic Lineage Reprogramming. *Cold Spring Harb Perspect Biol*, (2021).
32. H. M. Kang, M. Subramaniam, S. Targ, M. Nguyen, L. Maliskova, E. McCarthy, E. Wan, S. Wong, L. Byrnes, C. M. Lanata, R. E. Gate, S. Mostafavi, A. Marson, N. Zaitlen, L. A. Criswell, C. J. Ye, Multiplexed droplet single-cell RNA-sequencing using natural genetic variation. *Nat Biotechnol* **36**, 89-94 (2018).
33. E. Marron Fernandez de Velasco, L. Zhang, N. V. B, M. Tipps, S. Farris, Z. Xia, A. Anderson, N. Carlblom, C. D. Weaver, S. M. Dudek, K. Wickman, GIRK2 splice variants and neuronal G protein-gated K(+) channels: implications for channel function and behavior. *Sci Rep* **7**, 1639 (2017).

34. A. Cáceres, G. A. Banker, L. Binder, Immunocytochemical localization of tubulin and microtubule-associated protein 2 during the development of hippocampal neurons in culture. *J Neurosci* **6**, 714-722 (1986).
35. F. Ma, J. Xu, Y. Liu, D. Popova, M. M. Youssef, R. P. Hart, K. Herrup, The amyloid precursor protein modulates the position and length of the axon initial segment offering a new perspective on Alzheimer's disease genetics. *bioRxiv*, 2022.2001.2023.477413 (2022).
36. N. Wydeven, E. Marron Fernandez de Velasco, Y. Du, M. A. Benneyworth, M. C. Hearing, R. A. Fischer, M. J. Thomas, C. D. Weaver, K. Wickman, Mechanisms underlying the activation of G-protein-gated inwardly rectifying K+ (GIRK) channels by the novel anxiolytic drug, ML297. *Proc Natl Acad Sci U S A* **111**, 10755-10760 (2014).
37. E. Days, K. Kaufmann, I. Romaine, C. Niswender, M. Lewis, T. Utley, Y. Du, G. Sliwoski, R. Morrison, E. S. Dawson, J. L. Engers, J. Denton, J. S. Daniels, G. A. Sulikowski, C. W. Lindsley, C. D. Weaver, "Discovery and Characterization of a Selective Activator of the G-Protein Activated Inward-Rectifying Potassium (GIRK) Channel" in *Probe Reports from the NIH Molecular Libraries Program* (National Center for Biotechnology Information (US), Bethesda (MD), 2010).
38. T. W. Chen, T. J. Wardill, Y. Sun, S. R. Pulver, S. L. Renninger, A. Baohan, E. R. Schreiter, R. A. Kerr, M. B. Orger, V. Jayaraman, L. L. Looger, K. Svoboda, D. S. Kim, Ultrasensitive fluorescent proteins for imaging neuronal activity. *Nature* **499**, 295-300 (2013).
39. M. Steri, M. L. Idda, M. B. Whalen, V. Orrù, Genetic variants in mRNA untranslated regions. *Wiley Interdiscip Rev RNA* **9**, e1474 (2018).
40. D. Wang, S. Liu, J. Warrell, H. Won, X. Shi, F. C. P. Navarro, D. Clarke, M. Gu, P. Emani, Y. T. Yang, M. Xu, M. J. Gandal, S. Lou, J. Zhang, J. J. Park, C. Yan, S. K. Rhie, K. Manakongtreecheep, H. Zhou, A. Nathan, M. Peters, E. Mattei, D. Fitzgerald, T. Brunetti, J. Moore, Y. Jiang, K. Girdhar, G. E. Hoffman, S. Kalayci, Z. H. Gümüş, G. E. Crawford, P. Roussos, S. Akbarian, A. E. Jaffe, K. P. White, Z. Weng, N. Sestan, D. H. Geschwind, J. A. Knowles, M. B. Gerstein, Comprehensive functional genomic resource and integrative model for the human brain. *Science* **362**, (2018).
41. Y. O. Nunez, R. D. Mayfield, Understanding Alcoholism Through microRNA Signatures in Brains of Human Alcoholics. *Front Genet* **3**, 43 (2012).
42. C. Wehrspaun, C. Ponting, A. Marques, Brain-expressed 3′UTR extensions strengthen miRNA cross-talk between ion channel/transporter encoding mRNAs. *Frontiers in Genetics* **5**, (2014).
43. S. Suda, M. Nibuya, H. Suda, K. Takamatsu, T. Miyazaki, S. Nomura, N. Kawai, Potassium channel mRNAs with AU-rich elements and brain-specific expression. *Biochem Biophys Res Commun* **291**, 1265-1271 (2002).
44. K. Bodhinathan, P. A. Slesinger, Molecular mechanism underlying ethanol activation of G-protein-gated inwardly rectifying potassium channels. *Proc Natl Acad Sci U S A* **110**, 18309-18314 (2013).
45. P. Sathyan, H. B. Golden, R. C. Miranda, Competing interactions between micro-RNAs determine neural progenitor survival and proliferation after ethanol exposure: evidence from an ex vivo model of the fetal cerebral cortical neuroepithelium. *J Neurosci* **27**, 8546-8557 (2007).
46. A. Z. Pietrzykowski, R. M. Friesen, G. E. Martin, S. I. Puig, C. L. Nowak, P. M. Wynne, H. T. Siegelmann, S. N. Treistman, Posttranscriptional regulation of BK channel splice variant stability by miR-9 underlies neuroadaptation to alcohol. *Neuron* **59**, 274-287 (2008).

47. J. M. Lewohl, Y. O. Nunez, P. R. Dodd, G. R. Tiwari, R. A. Harris, R. D. Mayfield, Up-regulation of microRNAs in brain of human alcoholics. *Alcohol Clin Exp Res* **35**, 1928-1937 (2011).
48. E. A. Osterndorff-Kahanek, G. R. Tiwari, M. F. Lopez, H. C. Becker, R. A. Harris, R. D. Mayfield, Long-term ethanol exposure: Temporal pattern of microRNA expression and associated mRNA gene networks in mouse brain. *PLoS One* **13**, e0190841 (2018).
49. Y. Lim, J. E. Beane-Ebel, Y. Tanaka, B. Ning, C. R. Husted, D. C. Henderson, Y. Xiang, I. H. Park, L. A. Farrer, H. Zhang, Exploration of alcohol use disorder-associated brain miRNA-mRNA regulatory networks. *Translational psychiatry* **11**, 504 (2021).
50. S. Zhu, J. Wu, J. Hu, Non-coding RNA in alcohol use disorder by affecting synaptic plasticity. *Exp Brain Res*, (2022).
51. T. K. Best, R. J. Siarey, Z. Galdzicki, Ts65Dn, a mouse model of Down syndrome, exhibits increased GABAB-induced potassium current. *J Neurophysiol* **97**, 892-900 (2007).
52. C. Harashima, D. M. Jacobowitz, J. Witta, R. C. Borke, T. K. Best, R. J. Siarey, Z. Galdzicki, Abnormal expression of the G-protein-activated inwardly rectifying potassium channel 2 (GIRK2) in hippocampus, frontal cortex, and substantia nigra of Ts65Dn mouse: a model of Down syndrome. *J Comp Neurol* **494**, 815-833 (2006).
53. R. H. Reeves, N. G. Irving, T. H. Moran, A. Wohn, C. Kitt, S. S. Sisodia, C. Schmidt, R. T. Bronson, M. T. Davisson, A mouse model for Down syndrome exhibits learning and behaviour deficits. *Nat Genet* **11**, 177-184 (1995).
54. A. M. Kleschevnikov, J. Yu, J. Kim, L. V. Lysenko, Z. Zeng, Y. E. Yu, W. C. Mobley, Evidence that increased Kcnj6 gene dose is necessary for deficits in behavior and dentate gyrus synaptic plasticity in the Ts65Dn mouse model of Down syndrome. *Neurobiol Dis* **103**, 1-10 (2017).
55. E. Congdon, T. Canli, The endophenotype of impulsivity: reaching consilience through behavioral, genetic, and neuroimaging approaches. *Behav Cogn Neurosci Rev* **4**, 262-281 (2005).
56. D. M. Dick, G. Smith, P. Olausson, S. H. Mitchell, R. F. Leeman, S. S. O'Malley, K. Sher, Understanding the construct of impulsivity and its relationship to alcohol use disorders. *Addict Biol* **15**, 217-226 (2010).
57. K. J. Sher, T. J. Trull, Personality and disinhibitory psychopathology: alcoholism and antisocial personality disorder. *J Abnorm Psychol* **103**, 92-102 (1994).
58. A. Verdejo-García, A. J. Lawrence, L. Clark, Impulsivity as a vulnerability marker for substance-use disorders: review of findings from high-risk research, problem gamblers and genetic association studies. *Neurosci Biobehav Rev* **32**, 777-810 (2008).
59. J. Polich, F. E. Bloom, P300, alcoholism heritability, and stimulus modality. *Alcohol* **17**, 149-156 (1999).
60. U. Weissbein, M. Schachter, D. Egli, N. Benvenisty, Analysis of chromosomal aberrations and recombination by allelic bias in RNA-Seq. *Nature communications* **7**, 12144 (2016).
61. T. Vierbuchen, A. Ostermeier, Z. P. Pang, Y. Kokubu, T. C. Sudhof, M. Wernig, Direct conversion of fibroblasts to functional neurons by defined factors. *Nature* **463**, 1035-1041 (2010).
62. Z. P. Pang, N. Yang, T. Vierbuchen, A. Ostermeier, D. R. Fuentes, T. Q. Yang, A. Citri, V. Sebastiano, S. Marro, T. C. Sudhof, M. Wernig, Induction of human neuronal cells by defined transcription factors. *Nature* **476**, 220-223 (2011).
63. Y. Zhang, C. Pak, Y. Han, H. Ahlenius, Z. Zhang, S. Chanda, S. Marro, C. Patzke, C. Acuna, J. Covy, W. Xu, N. Yang, T. Danko, L. Chen, M. Wernig, T. C. Sudhof, Rapid single-step induction of functional neurons from human pluripotent stem cells. *Neuron* **78**, 785-798 (2013).

64. C. Bardy, M. van den Hurk, T. Eames, C. Marchand, R. V. Hernandez, M. Kellogg, M. Gorris, B. Galet, V. Palomares, J. Brown, A. G. Bang, J. Mertens, L. Bohnke, L. Boyer, S. Simon, F. H. Gage, Neuronal medium that supports basic synaptic functions and activity of human neurons in vitro. *Proc Natl Acad Sci U S A* **112**, E2725-2734 (2015).
65. N. Yang, S. Chanda, S. Marro, Y.-H. Ng, J. A. Janas, D. Haag, C. E. Ang, Y. Tang, Q. Flores, M. Mall, O. Wapinski, M. Li, H. Ahlenius, J. L. Rubenstein, H. Y. Chang, A. A. Buylla, T. C. Südhof, M. Wernig, Generation of pure GABAergic neurons by transcription factor programming. *Nature Methods* **14**, 621-628 (2017).
66. Y. Miyaoka, A. H. Chan, L. M. Judge, J. Yoo, M. Huang, T. D. Nguyen, P. P. Lizarraga, P. L. So, B. R. Conklin, Isolation of single-base genome-edited human iPS cells without antibiotic selection. *Nature methods* **11**, 291-293 (2014).
67. F. A. Ran, P. D. Hsu, J. Wright, V. Agarwala, D. A. Scott, F. Zhang, Genome engineering using the CRISPR-Cas9 system. *Nature Protocols* **8**, 2281-2308 (2013).
68. S. Chen, Y. Zhou, Y. Chen, J. Gu, fastp: an ultra-fast all-in-one FASTQ preprocessor. *Bioinformatics (Oxford, England)* **34**, i884-i890 (2018).
69. D. Kim, J. M. Paggi, C. Park, C. Bennett, S. L. Salzberg, Graph-based genome alignment and genotyping with HISAT2 and HISAT-genotype. *Nature Biotechnology* **37**, 907-915 (2019).
70. Y. Liao, G. K. Smyth, W. Shi, The R package Rsubread is easier, faster, cheaper and better for alignment and quantification of RNA sequencing reads. *Nucleic acids research* **47**, e47-e47 (2019).
71. M. I. Love, W. Huber, S. Anders, Moderated estimation of fold change and dispersion for RNA-seq data with DESeq2. *Genome Biol* **15**, 550 (2014).
72. A. Butler, P. Hoffman, P. Smibert, E. Papalexi, R. Satija, Integrating single-cell transcriptomic data across different conditions, technologies, and species. *Nat Biotechnol* **36**, 411-420 (2018).
73. C. A. Schneider, W. S. Rasband, K. W. Eliceiri, NIH Image to ImageJ: 25 years of image analysis. *Nature methods* **9**, 671-675 (2012).
74. S.-Y. Ho, C.-Y. Chao, H.-L. Huang, T.-W. Chiu, P. Charoenkwan, E. Hwang, NeurphologyJ: An automatic neuronal morphology quantification method and its application in pharmacological discovery. *BMC Bioinformatics* **12**, 230 (2011).
75. I. Arganda-Carreras, V. Kaynig, C. Rueden, K. W. Eliceiri, J. Schindelin, A. Cardona, H. Sebastian Seung, Trainable Weka Segmentation: a machine learning tool for microscopy pixel classification. *Bioinformatics* **33**, 2424-2426 (2017).
76. J. A. Fantuzzo, D. A. Robles, V. R. Mirabella, R. P. Hart, Z. P. Pang, J. D. Zahn, Development of a high-throughput arrayed neural circuitry platform using human induced neurons for drug screening applications. *Lab Chip* **20**, 1140-1152 (2020).
77. Z. M. Zhang, S. Chen, Y. Z. Liang, Baseline correction using adaptive iteratively reweighted penalized least squares. *Analyst* **135**, 1138-1146 (2010).
78. D. Bates, M. Mächler, B. Bolker, S. Walker, Fitting Linear Mixed-Effects Models Using lme4. *Journal of Statistical Software* **67**, 1 - 48 (2015).
79. S. Højsgaard, U. Halekoh, J. Yan, The R Package geepack for Generalized Estimating Equations. *Journal of Statistical Software* **15**, 1 - 11 (2005).

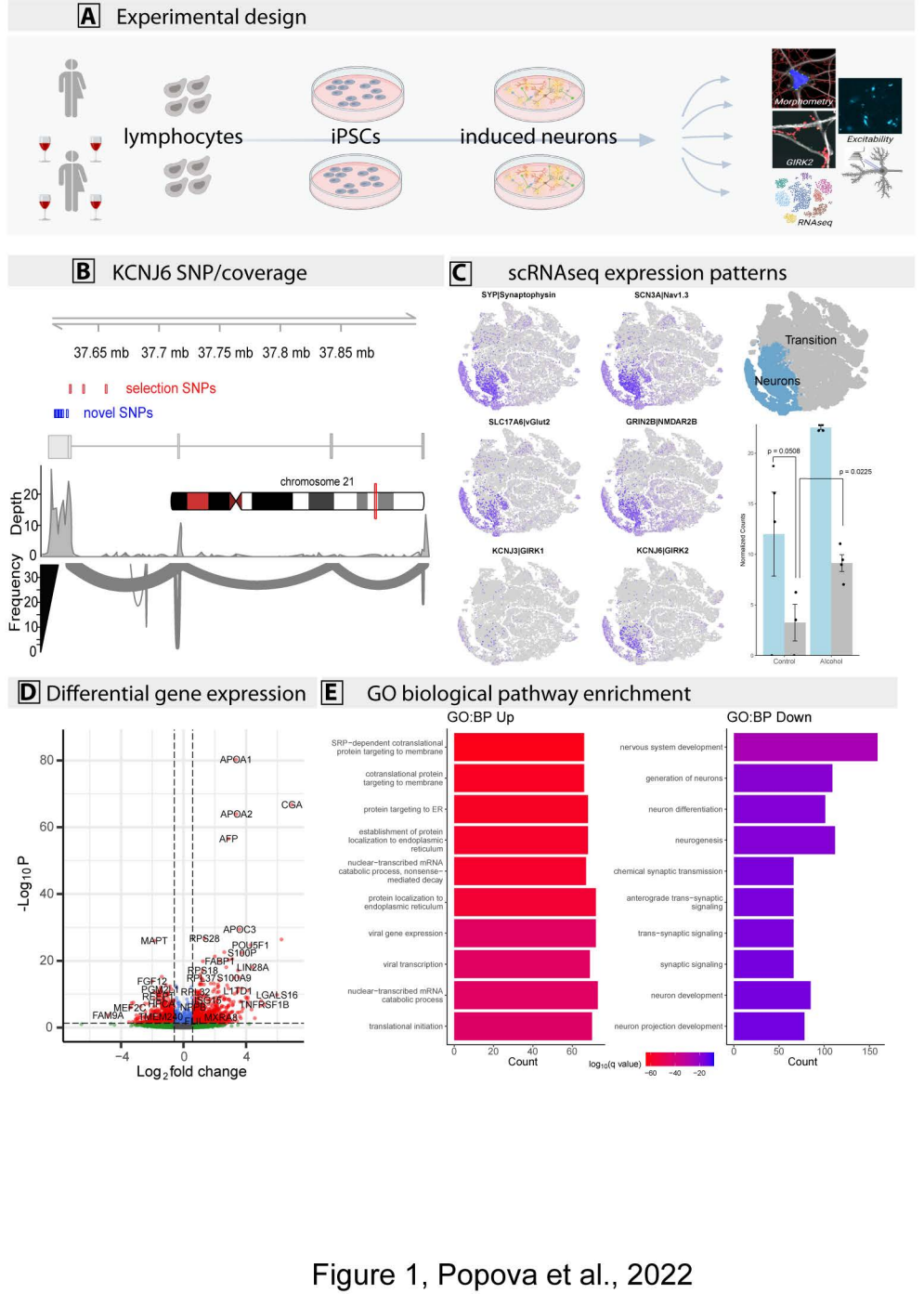

Figure 1, Popova et al., 2022

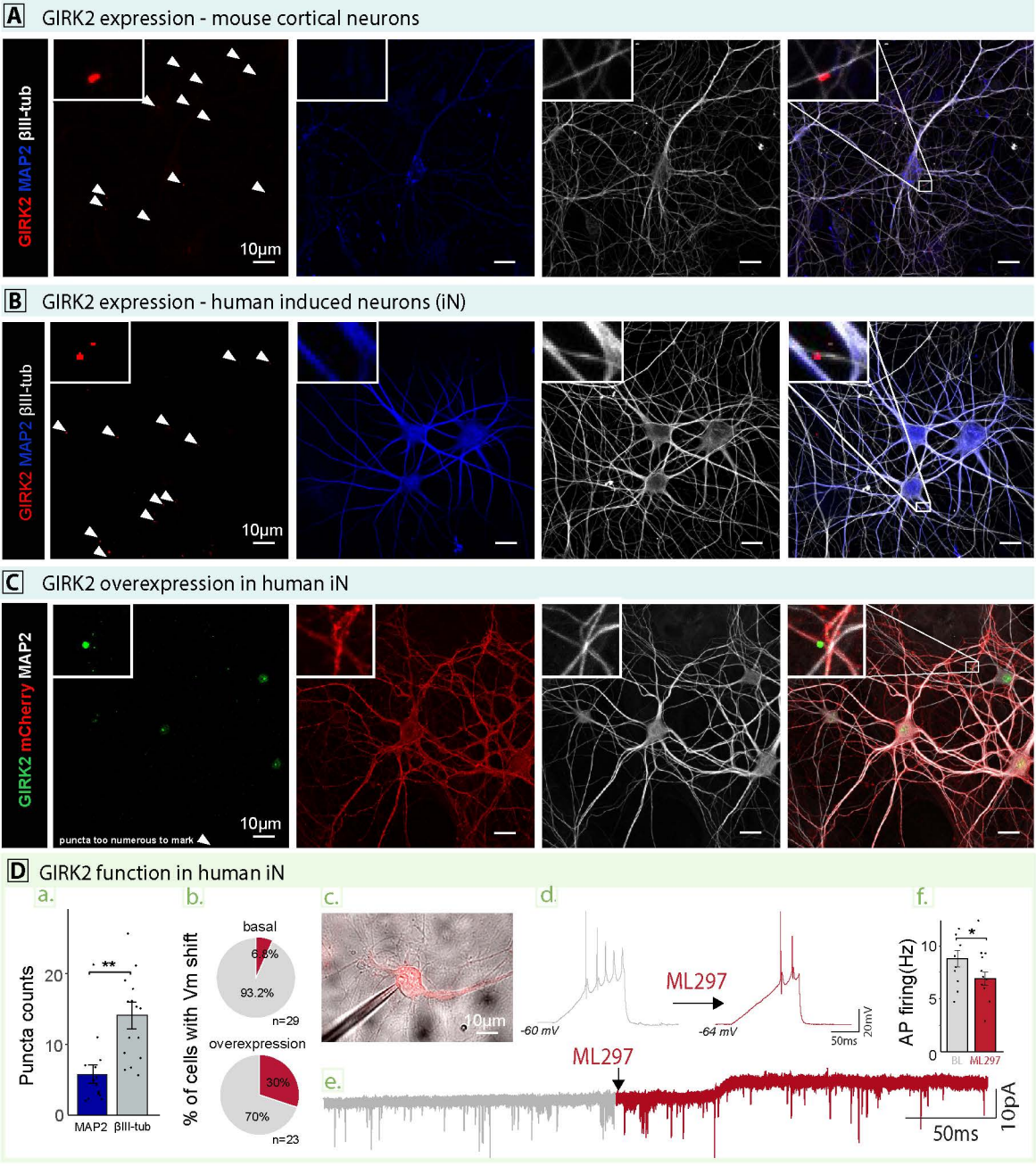

Figure 2, Popova et al., 2022

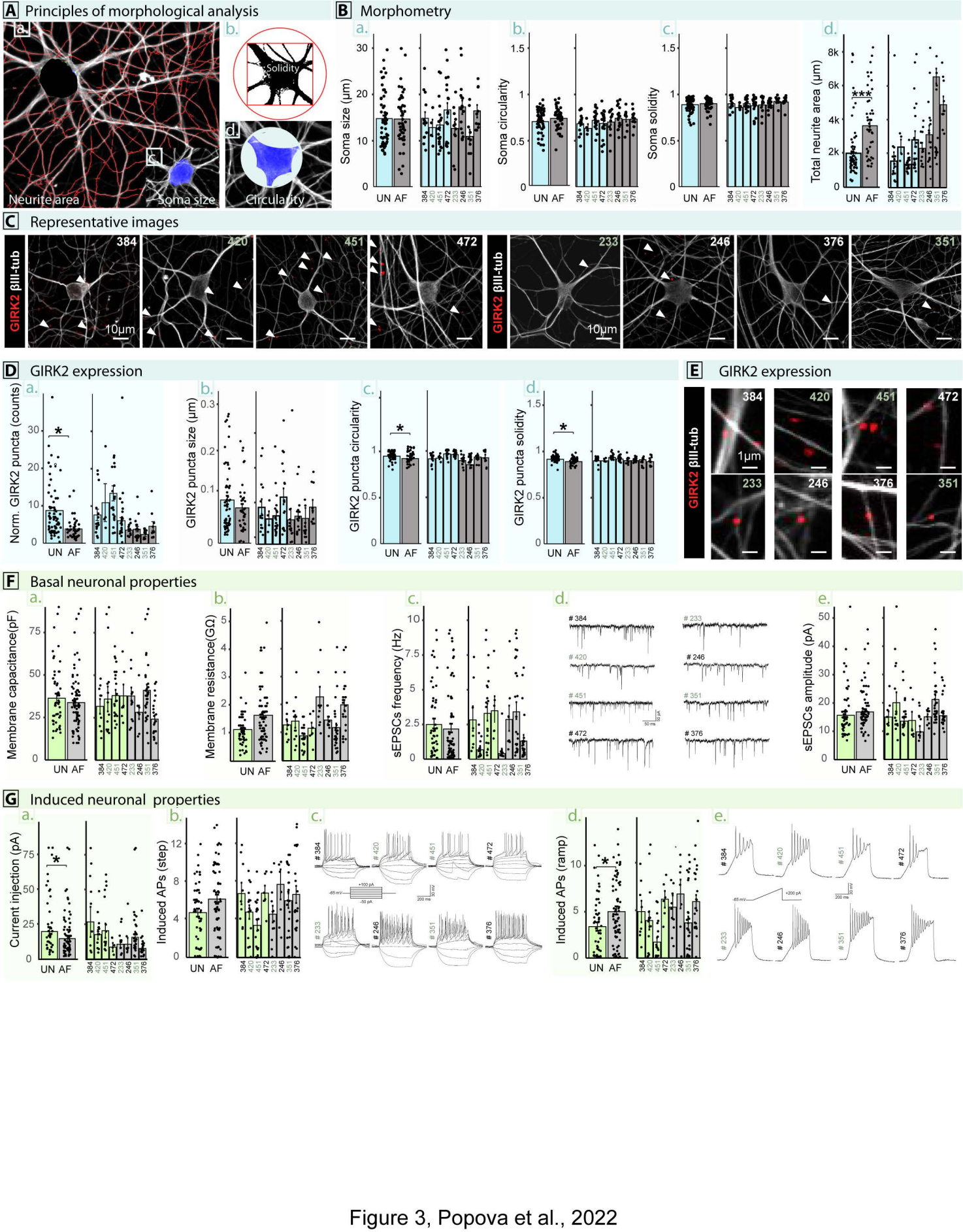

Figure 3, Popova et al., 2022

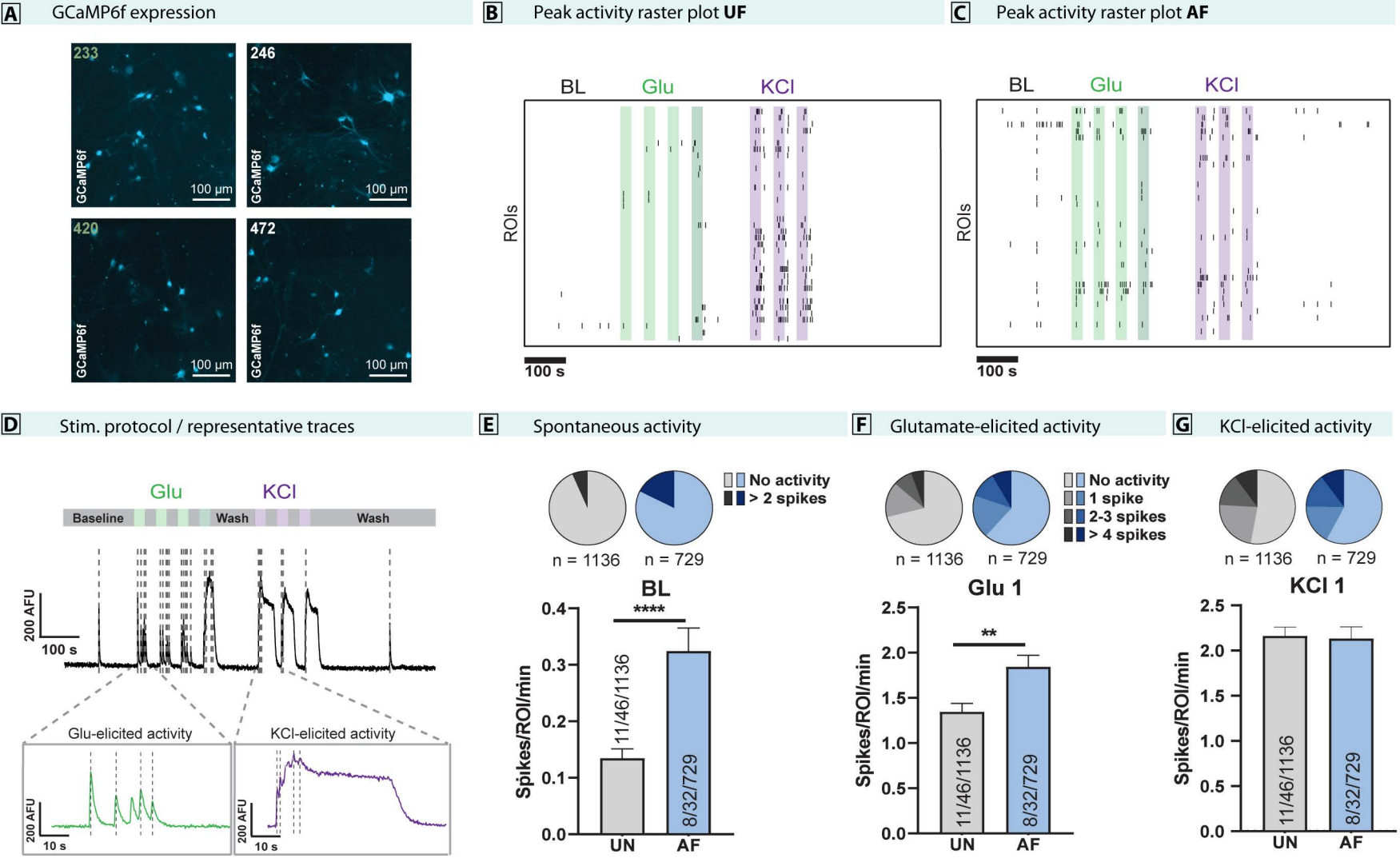

Figure 4, Popova et al., 2022

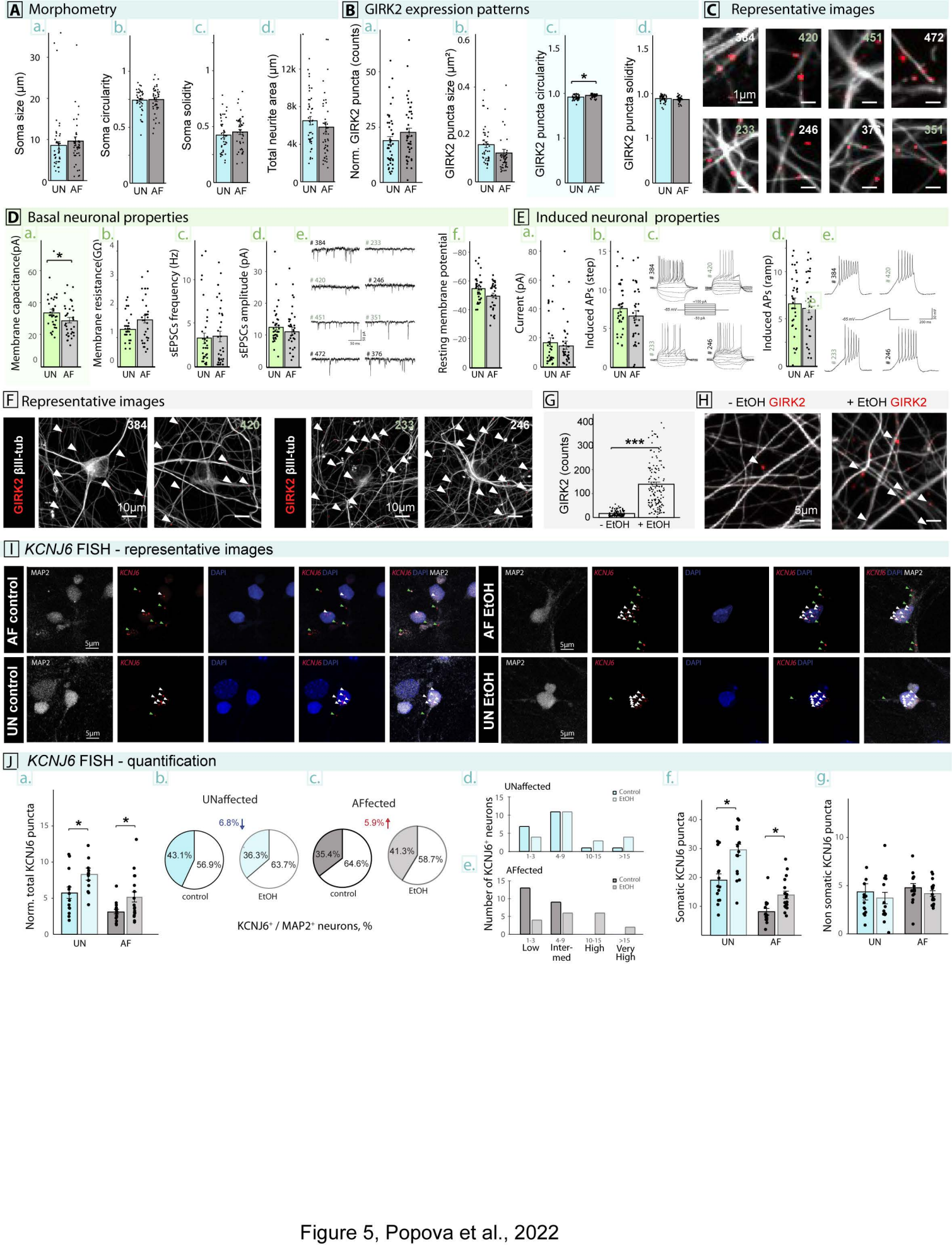

Figure 5, Popova et al., 2022

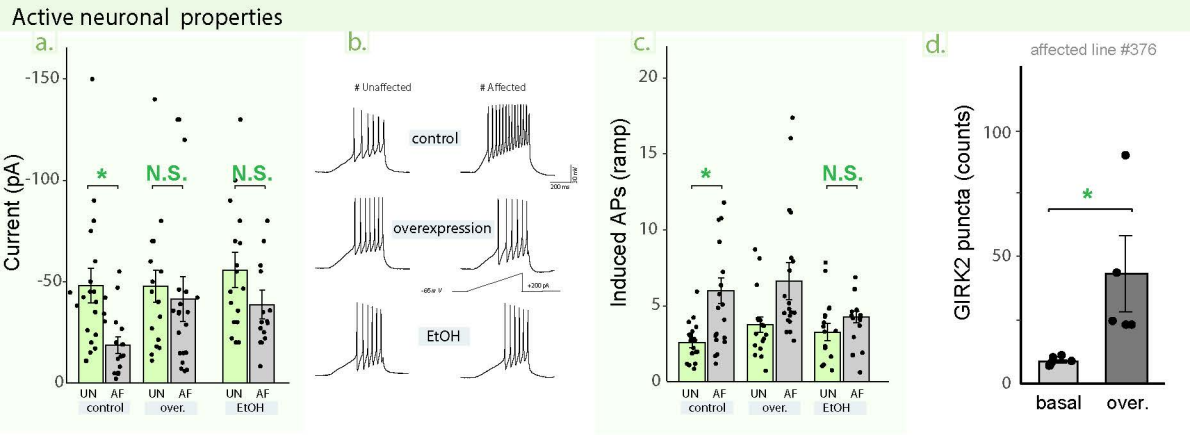

Figure 6, Popova et al., 2022